Defense Threat Reduction Agency
8725 John J. Kingman Road, MS
6201 Fort Belvoir, VA 22060-6201

DTRA-TR-16-55

TECHNICAL REPORT

Gadolinium-Based GaN for Neutron Detection with Gamma Discrimination

June 2016

HDTRA1-11-1-0013

Lei Cao, et al.

Prepared by:
The Ohio State University
E402, 201 W 19th Ave.
Columbus, Ohio 43210

DESTRUCTION NOTICE:

Destroy this report when it is no longer needed.
Do not return to sender.

PLEASE NOTIFY THE DEFENSE THREAT REDUCTION AGENCY, ATTN: DTRIAC/ J9STT, 8725 JOHN J. KINGMAN ROAD, MS-6201, FT BELVOIR, VA 22060-6201, IF YOUR ADDRESS IS INCORRECT, IF YOU WISH IT DELETED FROM THE DISTRIBUTION LIST, OR IF THE ADDRESSEE IS NO LONGER EMPLOYED BY YOUR ORGANIZATION.

REPORT DOCUMENTATION PAGE

Form Approved
OMB No. 0704-0188

1. REPORT DATE *(DD-MM-YYYY)*	**2. REPORT TYPE**	**3. DATES COVERED** *(From - To)*
00-06-2016	Technical	June 5, 2011 - September 30, 2013

4. TITLE AND SUBTITLE

Gadolinium-Based GaN for Neutron Detection with Gamma Discrimination

5a. CONTRACT NUMBER
HDTRA1-11-1-0013

5b. GRANT NUMBER

5c. PROGRAM ELEMENT NUMBER

6. AUTHOR(S)

Lei R. Cao, Padhraic L. Mulligan, Praneeth Kandlakunta, Jinghui Wang

5d. PROJECT NUMBER

5e. TASK NUMBER

5f. WORK UNIT NUMBER

7. PERFORMING ORGANIZATION NAME(S) AND ADDRESS(ES)

Nuclear Engineering Program
Department of Mechanical and Aerospace Engineering
The Ohio State University
201 W 19th Ave.
Columbus, OH 43210

8. PERFORMING ORGANIZATION REPORT NUMBER

9. SPONSORING / MONITORING AGENCY NAME(S) AND ADDRESS(ES)

Defense Threat Reduction Agency
8725 John J. Kingman Road, STOP 6201
Fort Belvoir, VA 22060-6201

10. SPONSOR/MONITOR'S ACRONYM(S)
DTRA

11. SPONSOR/MONITOR'S REPORT NUMBER(S)
DTRA-TR-16-55

12. DISTRIBUTION / AVAILABILITY STATEMENT

Distribution Statement A. Approved for public release, distribution is unlimited.

13. SUPPLEMENTARY NOTES

14. ABSTRACT

The objective of this project is to develop and understanding of the fundamental material electronics response from a gadolinium-based GaN semiconductor device exposed to neutron radiation. The GaN Schottky diode radiation sensor has been successfully fabricated and shown alpha and beta response. Neutron spectrum using 6Li as a converter was successfully obtained. To understand devices' electronic properties, the detector has been characterized by current-voltage, capacitance-voltage, charge collection efficiency, alpha spectroscopy, etc. In addition, numerical simulations using TCAD software have been performed to reveal the charge migration and to understand the fundamental material and device properties at picosecond scale. The proposed twin-detector design for gamma-ray discrimination was validated both theoretically and experimentally.

15. SUBJECT TERMS

neutron detection; gadolinium; gamma-ray; radiation detectors

16. SECURITY CLASSIFICATION OF:			**17. LIMITATION OF ABSTRACT**	**18. NUMBER OF PAGES**	**19a. NAME OF RESPONSIBLE PERSON**
					Dave Petersen
a. REPORT	**b. ABSTRACT**	**c. THIS PAGE**	SAR	61	**19b. TELEPHONE NUMBER** *(include area code)*
Unclassified	Unclassified	Unclassified			703-767-3164

Standard Form 298 (Rev. 8-98)
Prescribed by ANSI Std. Z39.18

UNIT CONVERSION TABLE

U.S. customary units to and from international units of measurement*

U.S. Customary Units	Multiply by → / ← Divide by†		International Units
Length/Area/Volume			
inch (in)	2.54	$\times 10^{-2}$	meter (m)
foot (ft)	3.048	$\times 10^{-1}$	meter (m)
yard (yd)	9.144	$\times 10^{-1}$	meter (m)
mile (mi, international)	1.609 344	$\times 10^{3}$	meter (m)
mile (nmi, nautical, U.S.)	1.852	$\times 10^{3}$	meter (m)
barn (b)	1	$\times 10^{-28}$	square meter (m^2)
gallon (gal, U.S. liquid)	3.785 412	$\times 10^{-3}$	cubic meter (m^3)
cubic foot (ft^3)	2.831 685	$\times 10^{-2}$	cubic meter (m^3)
Mass/Density			
pound (lb)	4.535 924	$\times 10^{-1}$	kilogram (kg)
unified atomic mass unit (amu)	1.660 539	$\times 10^{-27}$	kilogram (kg)
pound-mass per cubic foot (lb ft^{-3})	1.601 846	$\times 10^{1}$	kilogram per cubic meter (kg m^{-3})
pound-force (lbf avoirdupois)	4.448 222		newton (N)
Energy/Work/Power			
electron volt (eV)	1.602 177	$\times 10^{-19}$	joule (J)
erg	1	$\times 10^{-7}$	joule (J)
kiloton (kt) (TNT equivalent)	4.184	$\times 10^{12}$	joule (J)
British thermal unit (Btu) (thermochemical)	1.054 350	$\times 10^{3}$	joule (J)
foot-pound-force (ft lbf)	1.355 818		joule (J)
calorie (cal) (thermochemical)	4.184		joule (J)
Pressure			
atmosphere (atm)	1.013 250	$\times 10^{5}$	pascal (Pa)
pound force per square inch (psi)	6.984 757	$\times 10^{3}$	pascal (Pa)
Temperature			
degree Fahrenheit (^oF)	$[T(^oF) - 32]/1.8$		degree Celsius (^oC)
degree Fahrenheit (^oF)	$[T(^oF) + 459.67]/1.8$		kelvin (K)
Radiation			
curie (Ci) [activity of radionuclides]	3.7	$\times 10^{10}$	per second (s^{-1}) [becquerel (Bq)]
roentgen (R) [air exposure]	2.579 760	$\times 10^{-4}$	coulomb per kilogram (C kg^{-1})
rad [absorbed dose]	1	$\times 10^{-2}$	joule per kilogram (J kg^{-1}) [gray (Gy)]
rem [equivalent and effective dose]	1	$\times 10^{-2}$	joule per kilogram (J kg^{-1}) [sievert (Sv)]

*Specific details regarding the implementation of SI units may be viewed at http://www.bipm.org/en/si/.

†Multiply the U.S. customary unit by the factor to get the international unit. Divide the international unit by the factor to get the U.S. customary unit.

Final Technical Report

BRBAA08-Per5-Y-1-2-0030

Title: "Gadolinium-Based GaN for Neutron Detection with Gamma Discrimination"

Grant number: HDTRA1-11-1-0013

Principal Investigator

Prof. Lei Cao

The Ohio State University

E402, 201 W 19th Ave.

Columbus, Ohio 43210

Phone: 614-247-8701

E-Mail: cao.152@osu.edu

Project effective date: May 26th, 2011

Project end date: September 30th, 2013

Contents

1. Summary 3
2. Device Fabrication 6
   2.1 Device Fabricated on Normal Growth GaN 6
   2.2 Device Fabricated on Special Growth GaN 7
3. Device Characterization 9
   3.1 Current-Voltage 9
   3.2 Capacitance-Voltage 10
4. Radiation Response 12
   4.1 Alpha Particle Spectra from Normal Growth GaN 12
   4.2 Neutron Spectra from Normal Growth GaN 13
   4.3 Alpha Particle Spectra from Special Growth GaN 15
   4.4 Beta Particle Spectra from Special Growth GaN 16
   4.5 Dual Detector Operation 17
5. Device Simulation 21
   5.1 Physical Models 21
   5.2 Comparison of Simulation and Experiment Results 23
   5.3 Transient Current Analysis 23
6. Gamma-ray Discrimination 28
   6.1 Gamma-ray Discrimination Scheme 28
   6.2 Experiment Setup 30
   6.3 Performance of Gd Covered Si Detector at Low Reactor Power 31
   6.4 Performance of Gd Covered Si Detector at High Reactor Power 33
   6.5 Performance of LiF Thin Film Covered GaN Twin-detector 34
7. Conclusions 38

References 42

Appendix 1: TCAD code for structure construction 44

Appendix 2: TCAD Code for I-V Simulation 46

Appendix 3: TCAD Code for C-V Simulation 48

Appendix 4: TCAD Code for Transient Current Simulation 51

Appendix 5: TCAD Code for Carrier Concentration Simulation 54

1. Summary

The objective of this project is to develop a gadolinium-based GaN semiconductor device for neutron detection in a radiation environment with ability to reject gamma-ray background. Aiming at this objective, several goals have been accomplished during the past years' research.

Workable GaN Schottky diode radiation detectors were successfully fabricated and tested. The first year has, however, seen a significant effort towards fabricating a working GaN radiation detector. One such detector design utilized semi-insulating GaN [1], sandwiched between ohmic and Schottky contacts. The Mg dopant added during the GaN ammonothermal growth resulted in deep level traps, and an alpha-particle response was not observed. A second detector design, consisting of a Schottky-ohmic mesa structure on a molecular beam epitaxy (MBE) grown super-lattice Gd:GaN, also failed to show radiation response due to prohibitively high leakage current [2].

The breakthrough was made in the second year when a Hydride Vapour Phase Epitaxy (HVPE) grown GaN substrate (Kyma technology [3]) was employed and the sandwich structure Schottky diode was fabricated, on which both alpha and neutron response were successfully obtained [4]. Due to wafer's high dislocation density, these detectors have a relatively high leakage current which hindered their ability for radiation detection. Finally, a n-type HVPE GaN substrate characterized by low carrier concentration and low dislocation density was obtained, detectors fabricated on which showed both alpha (^{241}Am source), beta (^{14}C source), and neutron response. The high signal-to-noise ratio guarantees their capability for neutron detection by employing Gd as a neutron converter.

To further understand the fundamental material electronic properties of these detectors, current-voltage (IV), capacitance-voltage (CV), and alpha spectroscopy measurement were performed and basic parameters were derived, such as the carrier concentration, Schottky barrier height, depletion region depth, and charge collection efficiency (CCE) etc. In addition, numerical simulations were carried out by using Sentaurus TCAD software package[5], which helped us to gain a deep insight into the charge collection process within the detector.

Parallel to these researches and findings, the proposed Gd thin-film covered twin-detector design for neutron detection was first validated by testing with Si detectors. The key feature of the design is using a polyethylene layer as the internal conversion electrons (ICE) separator. Radiation tests at both low and high neutron flux indicated that one detector generates a combined signal induced by both neutrons and gamma rays, whereas the other one produces a signal induced only by gamma rays. Thus a net signal that was introduced solely by neutrons can be obtained by subtracting the two signals. This concept was further validated by using GaN detector with ^{6}Li as a neutron converter. The experiment by employing Gd converter and polyethylene separator on GaN twin-detector device has also been performed, and thus the ultimately objective of this project is reached.

Three graduate students have dedicated to this project, and their research efforts culminated the production of two MS theses, and one PhD thesis. In Padhraic Muligan's thesis[6], a multi-detector digital neutron depth profiling instrument was designed and constructed in The Ohio State University Reactor Lab (OSURR) for neutron detections, in Jinghui Wang's thesis[7], the Schottky diode on GaN was successfully fabricated; in

Dr. Praneeth Kandlakunta's thesis[8], the twin-detector scheme was proposed and evaluated. In addition, seven peer-reviewed journal papers have been published [4, 9-14] and two are currently under preparation [15, 16], eight conference papers have published in proceedings[2, 13, 17-22], and a number of presentations have been delivered in various communities. The experiences working on this project enhanced students' abilities to undertake scientific researches and have shaped the directions of their further academic career.

2. Device Fabrication

2.1 Device Fabricated on Normal Growth GaN

During the past two years, GaN detectors have been fabricated on different types of semiconductors (semi-insulating, n-type) by employing various structures (mesa, sandwich [4], and super-lattice [2]). Experiences learned from evaluating these detectors are summarized as, 1) semi-insulating GaN [1] does not show radiation response due to the high density carrier trapping centers caused by Mg dopant; 2) Gd doped supper-lattice GaN is hindered by its high leakage current due to the large amount of dislocations formed during growth process; 3) the one fabricated on n-type GaN has shown both alpha and neutron response[1].

Figure 1 shows the sandwich structure radiation sensors constructed on freestanding n-type GaN wafers procured from Kyma Technologies Inc. The 1 cm × 1 cm wafers were sliced from a bulk GaN boule grown via Hydride Vapor Phase Epitaxy (HVPE), and subsequently polished to a nominal 475 μm thickness. A full-backside ohmic contact (Ti/Al/Ni/Au) was deposited on the N-face of the wafer using electron beam evaporation and a shadow mask. Several circular Schottky diodes (Ni/Au) with concentric guard rings were then deposited on the Ga-face by way of photolithography. The wafer was mounted in a Dual Inline Package (DIP) using Ag paste, and the Schottky diodes were wire bonded to the DIP bonding leads with 25-μm Au wire. The device was fabricated in Nanotech West Laboratory, The Ohio State University. The employed nanofabrication processes and the related facilities are listed in Table 1.

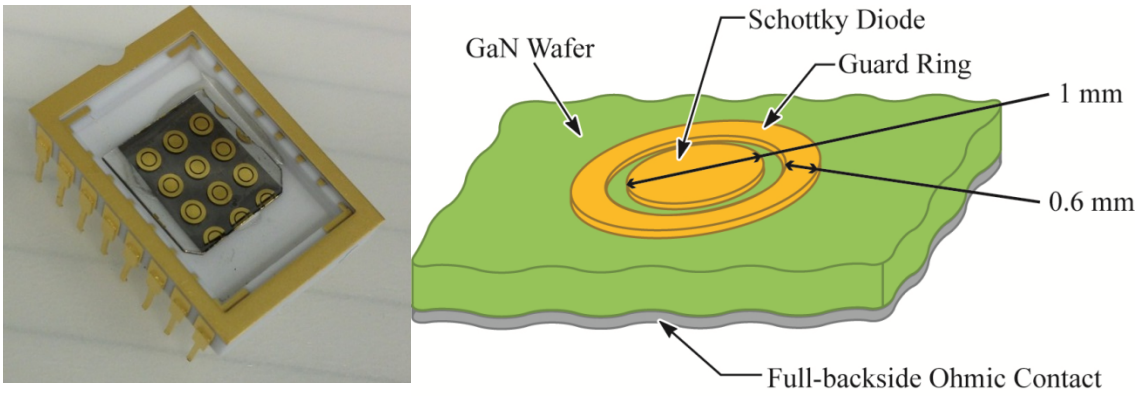

Figure 1. GaN wafer with nine Schottky diodes deposited on the Ga-face, mounted in DIP (left). Schematic of single GaN Schottky diode and guard ring with device dimensions, not to scale (right).

Table 1. Nanofabrication processes for GaN radiation detector fabrication

Nanofabrication process	**Facility**
Photomask design	L-Edit 7.12
Photolithography	EV 620 Aligner (ALN02)
Asher	Diener Pico Oxygen Plasma Asher (ASH01)
Etching	Plasma Therm 770 SLR ICP-RIE system (ETC04)
Metal Deposition	CHA Solution System E-Gun Evaporator (EVP03)
Rapid Thermal Annealing	AG Associates Model 410 Rapid Thermal Annealer (RTA01)
Wire Bonding	Kulicke and Soffe 3123 Wire Bonder (BND03)

2.2 Device Fabricated on Special Growth GaN

In order to improve the performance of our GaN detectors, several batches of detectors were fabricated on a specially grown HVPE n-type substrate purchased from Kyma technology [3], which was characterized by its low carrier concentration (~10^{14} cm^{-3}) and low dislocation density [23]. The parameters used for the growth of this material are currently unknown by our group for proprietary reasons. These substrates were specifically requested after a different group published successful results using similar material (hereafter referred to by its production number 1669) [23]. To utilize as much of the limited special growth GaN as possible, 1 mm diameter diodes with concentric guard rings were deposited on the wafer, followed by deposition of 0.5 mm diameter diodes in the open areas, see Figure 2.

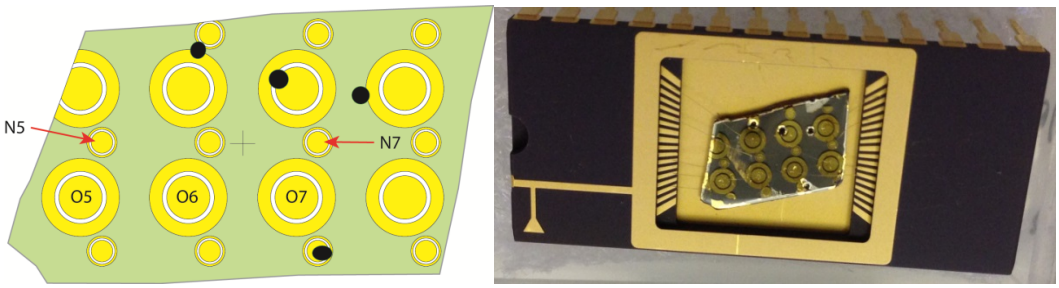

Figure 2. (Left) schematic of diode placement on special growth GaN wafer 1669. (Right) image of GaN wafer with diodes deposited.

3. Device Characterization

3.1 Current-Voltage

The current-voltage (IV) characteristic of the fabricated detectors on n-type GaN was performed by using a Keithley 2400 SourceMeter, all of which show considerable improvement in leakage current compared to the first year fabricated devices. The diodes fabricated on the special growth substrate showed a substantial decrease in current density when reverse biased. Additionally, the diodes could be biased to much higher voltages without approaching the breakdown voltage of the material. The special growth material also produced more successful diodes (5 total) than the previously utilized material (only 1). As Figure 3 indicates, the I-V measurements of one of these devices show leakage currents as low as 0.1nA constantly through a large reverse bias region. This level of leakage current is comparable with commercially available Si detector and is capable of producing high quality spectrometry.

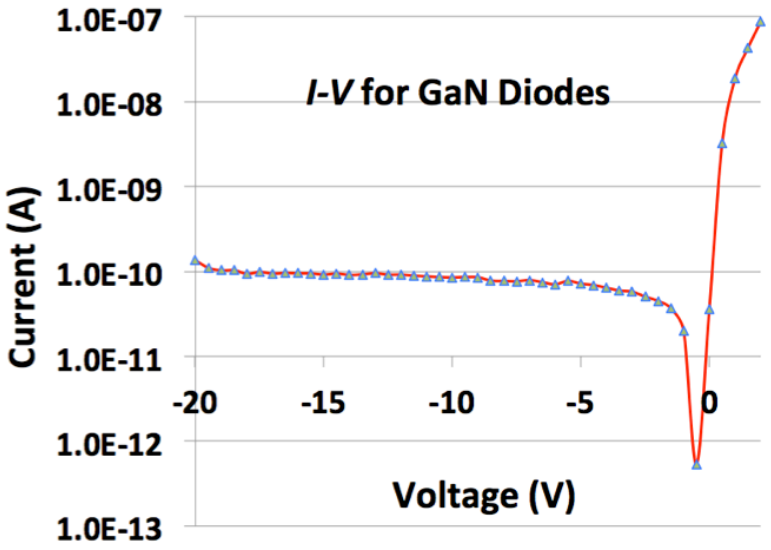

Figure 3. I-V measurement of one Schottky diode.

3.2 Capacitance-Voltage

C-V measurements using a 1 MHz Boonton 7200 capacitance meter on the n-type GaN wafer also showed a slightly lower carrier concentration in some diodes (9.57×10^{15} cm^{-3}) than the detectors fabricated on the standard HVPE material (1.65×10^{16} cm^{-3}). One of the diodes on the special growth material indicated an increased Schottky barrier height, which could be attributed to improvements in our surface cleaning methods prior to metallization.

Table 2. Diode Parameters Extracted from C-V Profiling

	Special Growth Wafer			Standard Wafer
Diode Number	1669-N7	1669-O5	1669-O7	2172-F7
Doping (cm^{-3})	2.06×10^{16}	2.31×10^{16}	9.57×10^{15}	1.65×10^{16}
Schottky Barrier Height (V)	1.29	1.04	1.08	1.04

Using the parameters obtained from C-V profiling of the detectors, the depletion depth in the detector as a function of reverse bias was calculated assuming an abrupt junction approximation. The results indicate two of the diodes on the special growth wafer have depletion depths quite similar to that of the standard wafer. One of the diodes on the special growth material had a slightly larger depletion depth, 2.28 µm at -50 V, compared to a maximum of 1.74 µm for the standard material. Although the gain in depletion depth by using the special growth material was not considerable, the reduction in leakage current was certainly beneficial to device performance. This became evident when testing the radiation sensitivity of the detectors using alpha and beta particle sources.

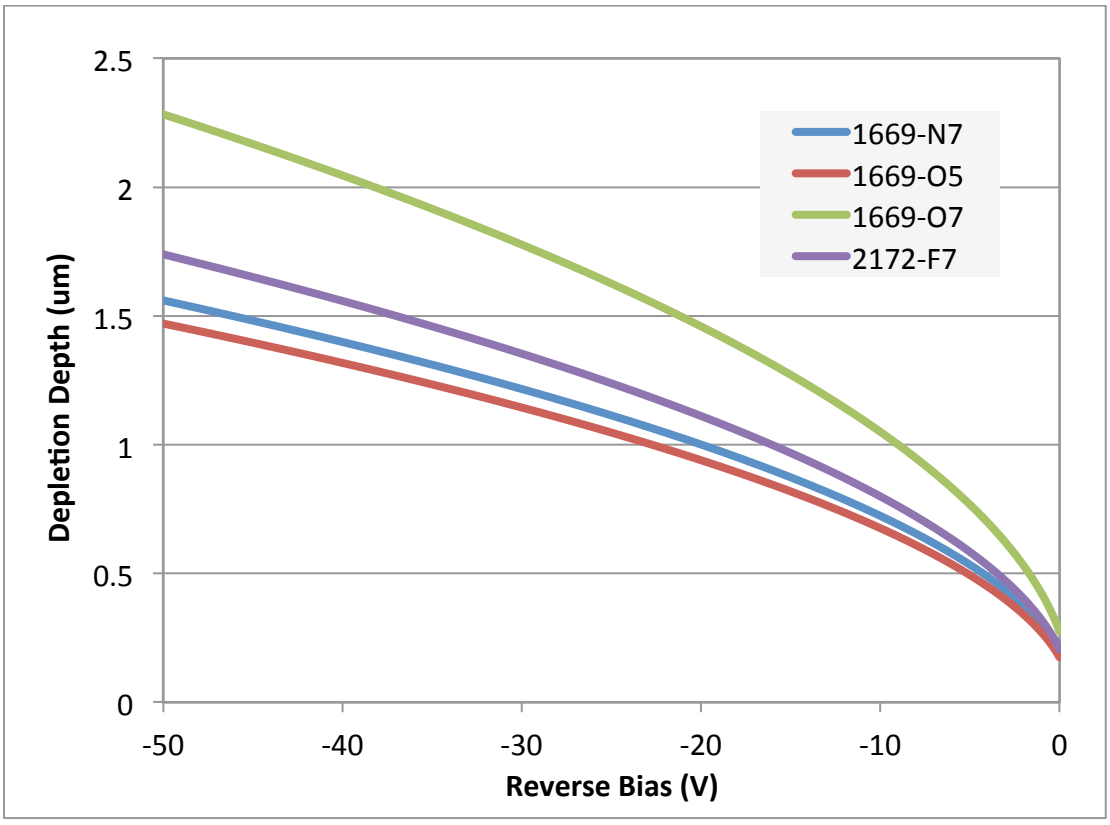

Figure 4. Depletion depth of diodes on special growth and standard GaN wafers as a function of reverse bias. Generated assuming an abrupt junction approximation using values derived from C-V measurements at room temperature.

4. Radiation Response

4.1 Alpha Particle Spectra from Normal Growth GaN

The experimental setup of the alpha spectroscopy system is shown in Figure 5, a vacuum chamber is used to minimize the particles' energy loss between the source and the detector, and at the same time its functions as an electromagnetic shield to reduce noise.

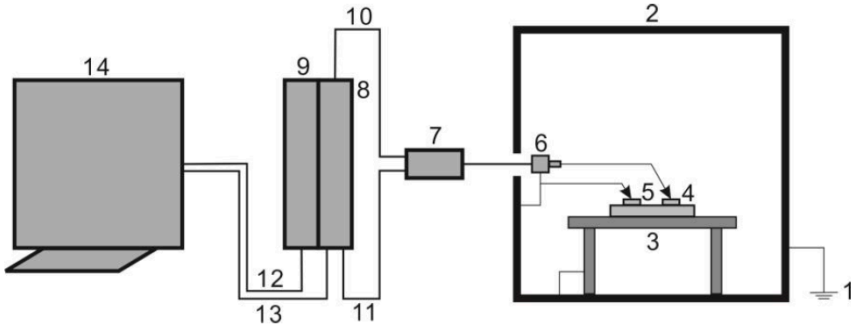

Figure 5. Alpha spectroscopy system: 1, Earth ground; 2, Shielding and vacuum chamber; 3, Probe station; 4, Ohmic contact; 5, Schottky Contact; 6, BNC cable; 7, Preamplifier; 8, CAEN N6724 Digitizer; 9, CAEN Power Supply; 10, Power supply to Preamplifier; 11, High voltage supply to detector; 12, Remote control of power supply; 13, Digitizer connect to computer; 14, Computer.

The initial radiation sensitivity of the sensor fabricated on the normal growth GaN was first tested using alpha particles. The GaN detectors, mounted in a DIP, were placed 1.5 cm below a 0.8 μCi ^{241}Am source in a vacuum chamber. The detectors were reverse biased by applying a positive potential to the ohmic contact and grounding the diode. Signals generated in the detector were collected by a 90 mV/MeV charge sensitive preamplifier, and digitized by a CAEN S.p.A. 100 Msample/s, 14-bit digitizer. Firmware in the digitizer provided a trapezoidal filter for the digitized signal, and was subsequently histogrammed. The collection efficiency of the device was investigated by sweeping the bias from 0 to 18 V. Results of the alpha spectrum are featured below in Figure 6.

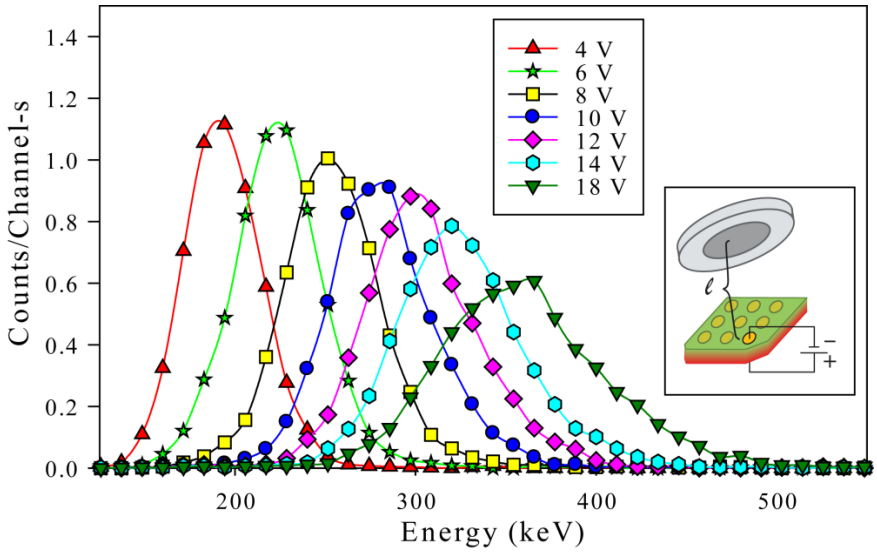

Figure 6. Alpha spectrum from 241Am source for a range of bias voltages. Inset figure is simple schematic for detector testing, with l = 1.5 cm.

As the figure indicates, increasing the detector bias resulted in a shift of the alpha peak to higher energies. This is to be expected as the 5.48 MeV alpha particle has a range of 14.4 μm as predicted by SRIM, far beyond the ~ 1 μm Space Charge Region (SCR) generated under these voltages. By increasing the bias voltage, and thus the SCR, more electron-hole pairs are generated in the SCR per incident particle. This results in a larger charge collected by the detector, and a larger voltage pulse from the preamp. The broadened peaks for larger biases also indicate some charge fails to be collected by the detector, due to the inclusion of more trapping centers in the larger SCR.

4.2 Neutron Spectra from Normal Growth GaN

To explore the feasibility of GaN as a neutron detection device, the detector was tested at the Ohio State University Research Reactor (OSURR) neutron beam facility. The beam facility is composed of a neutron collimator, to filter fast neutrons and shape the beam, a beam shutter, a vacuum chamber, and a sample mount for neutron sensitive material. The 450 kW light water reactor provides a 8.6×10^6 n/cm^2-s neutron flux to the

sample mount in the facility. The detector was placed several centimeters below the neutron beam, facing a 0.5 mm thick, 1.5 cm × 1.5 cm sample of oxidized natural Li (7.5% ^{6}Li), as shown in Figure 7. The Li_2O sample was mounted behind a polytetrafluoroethylene (PTFE) sheet with a 1 cm diameter aperture centered in the neutron beam.

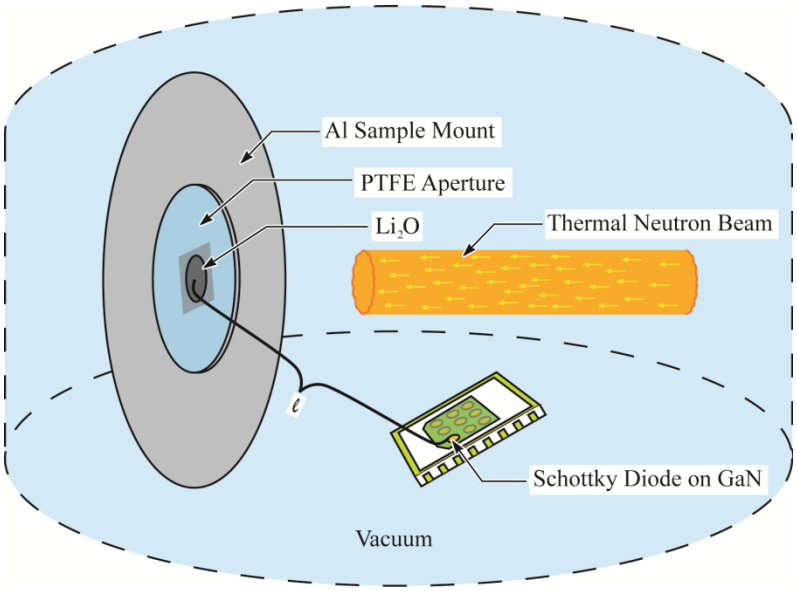

Figure 7. Simplified schematic of GaN neutron detection experiment, not to scale. l = 10.4 cm.

Figure 8 indicates that the sensor fabricated on normal growth GaN could detect charged particles induced by neutron absorption in ^{6}Li. Triton and alpha particles formed a peak in the GaN detector at rather low energies, which is to be expected considering the small SCR in the detector. Although a significant, low-energy background component was present, the neutron signal was substantially larger in the detector. While using a high-flux neutron source for testing may seem unconventional, considering the fact that the spectrum was obtained with a thermal neutron flux in the order of 10^{6} n/cm^{2}-s, the experimental setup also yielded a small detector solid angle, counteracting the high flux

used to test the device. Simulations performed using MCNP indicate the solid angle for the GaN detector in this experiment was (1.26±0.12) × 10^{-4} sr. As such, with the count rate achieved in this test, it is reasonable to consider the use of this device for low-level field applications, such as nuclear materials detection.

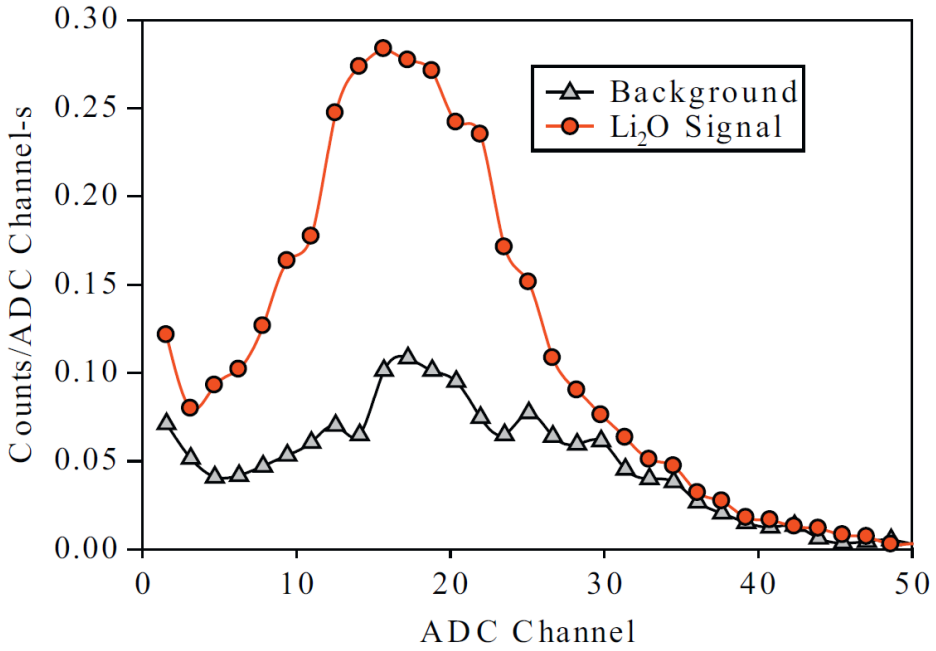

Figure 8. Neutron induced signal detected by GaN detector and neutron beam background.

4.3 Alpha Particle Spectra from Special Growth GaN

Spectra from all working diodes on the special growth wafer can be seen below in Figure 9. All diodes were initially reverse biased to 30 V. Leakage current for all diodes was between 5 and 10 nA at this voltage. As the figure shows, the smaller 0.5 mm diameter diodes N5 and N7 exhibit sharp peaks, with total efficiencies less than the larger diodes on the wafer. The centroid of N7 appears in a higher channel than that of N5, possibly indicating the depletion region of N7 is deeper than N5, resulting in more energy collected in the detector. The difference in peak area between detectors N5 and N7 (3.65 cps for N5 vs. 2.29 cps for N7) is primarily due to the difference in source-detector

distance and orientation between acquisitions. The same reasoning can explain the discrepancy in curve area between detectors O5, O6, and O7.

The two peaks appearing in the O5 and O6 spectra were deemed artificial because these peaks do not appear to correlate with any detection signal, and could be due to noise or signal reflection due to impedance mismatch in the detector. Detector O7 seemed somewhat promising for beta detection, given its single peak with a relatively high centroid.

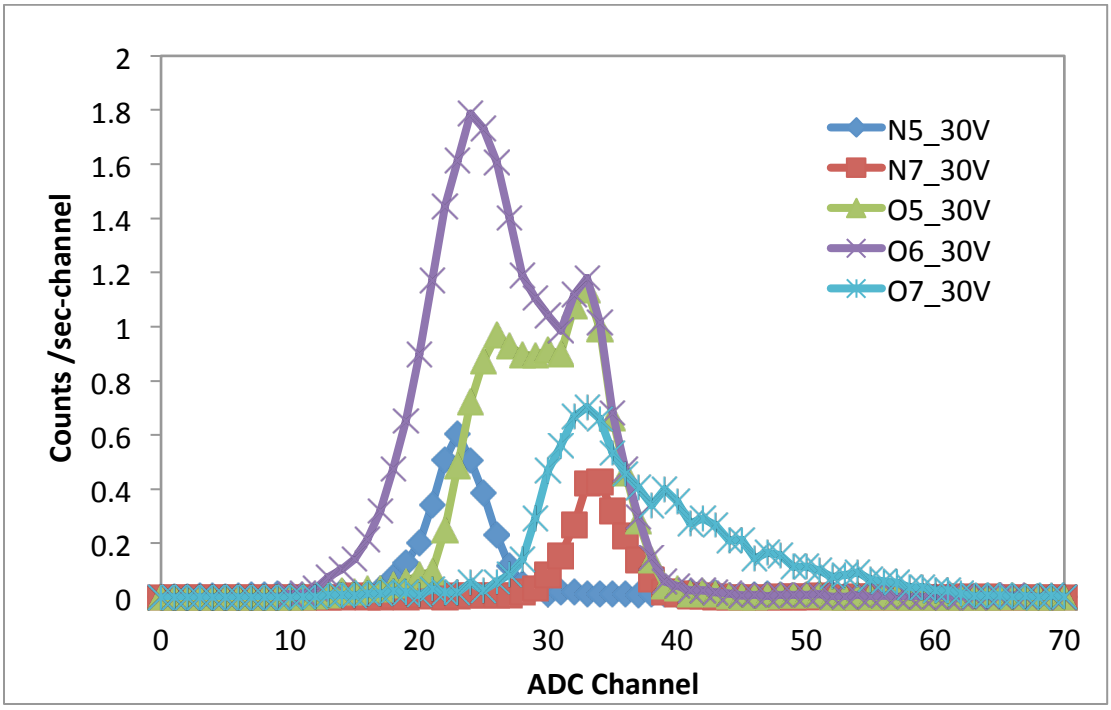

Figure 9. Am-241 spectra from operational diodes on wafer.

4.4 Beta Particle Spectra from Special Growth GaN

Collection of spectra from beta particles was also attempted on the new diodes since the proposed neutron convertor is Gd, which emits fast electrons upon neutron capture. Diode N7 appeared to show a good response to a ^{14}C source (E_{MAX} = 156 keV, E_{AVE} =

49.47 keV), as shown in Figure 10. The peak centered about channel 2 has a much higher count rate than the two reference background spectra. While it may appear strange that the background peak at low energy in Figure 10 do not appear in the spectra for ^{241}Am above, it should be noted that the lower detection threshold in the digital pulse processing software was lowered to accommodate the low energy beta particles. Beta spectra in other diodes were not as promising. The results indicates that not only did the background appear at a greater count rate than with the source presents, but the spectra appears to decrease in intensity over subsequent acquisitions, indicating a stability problem with those detectors.

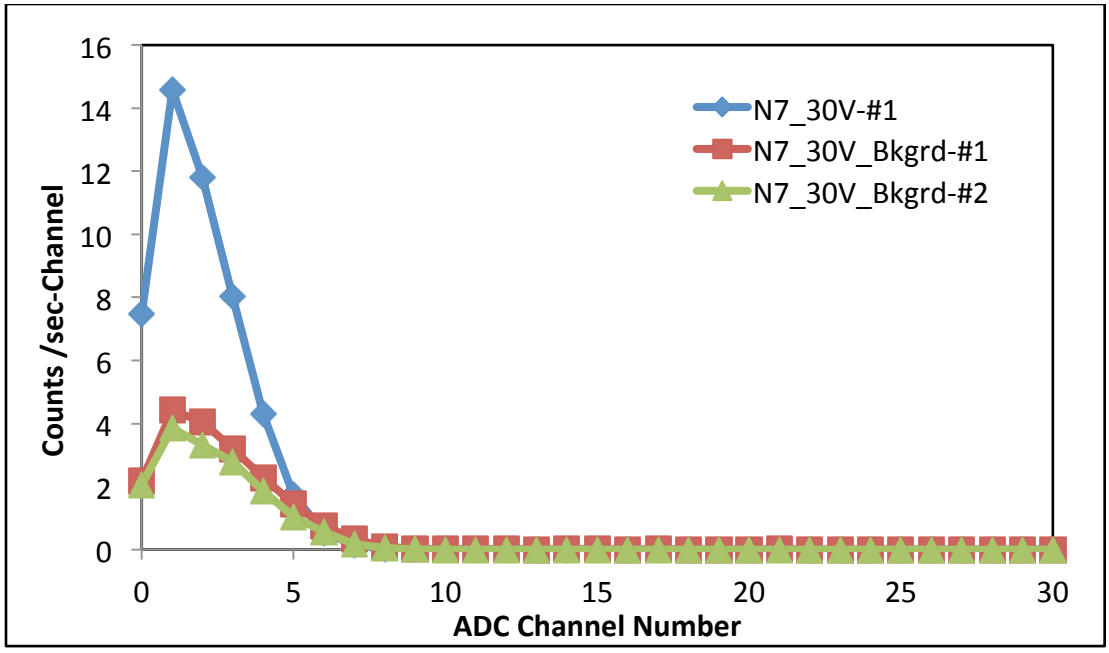

Figure 10. Beta spectra in detector N7 when reverse biased at 30 V.

4.5 Dual Detector Operation

One of the goals of this work is to create a neutron detector insensitive to gamma rays. One method of creating such a device is to subtract the signal of a neutron insensitive detector from a similar neutron sensitive detector, effectively reducing gamma

induced events. Since our fabrication process creates multiple detectors on a single wafer, we can use two or more devices simultaneously, without dicing the wafer. Subjecting the wafer to a dicing procedure could impart residual stress to the wafer, degrading the device's performance. To achieve this goal, I-V measurements were repeated while biasing two detectors simultaneously. Figure 11 shows I-V measurements taken from both diodes simultaneously, in comparison with I-V measurements obtained from each diode one at a time. Results indicate that one of the diodes (O5) begins to break down at a much lower voltage (-30 V vs. -43 V) when a second diode on the wafer is also reverse biased. Similarly, diode N7 has a slightly higher leakage current for reverse bias greater than -40 V if there is a second diode also biased on the wafer. Results from these experiments helped determine the appropriate voltage for each diode when collecting an alpha spectrum from both detectors simultaneously.

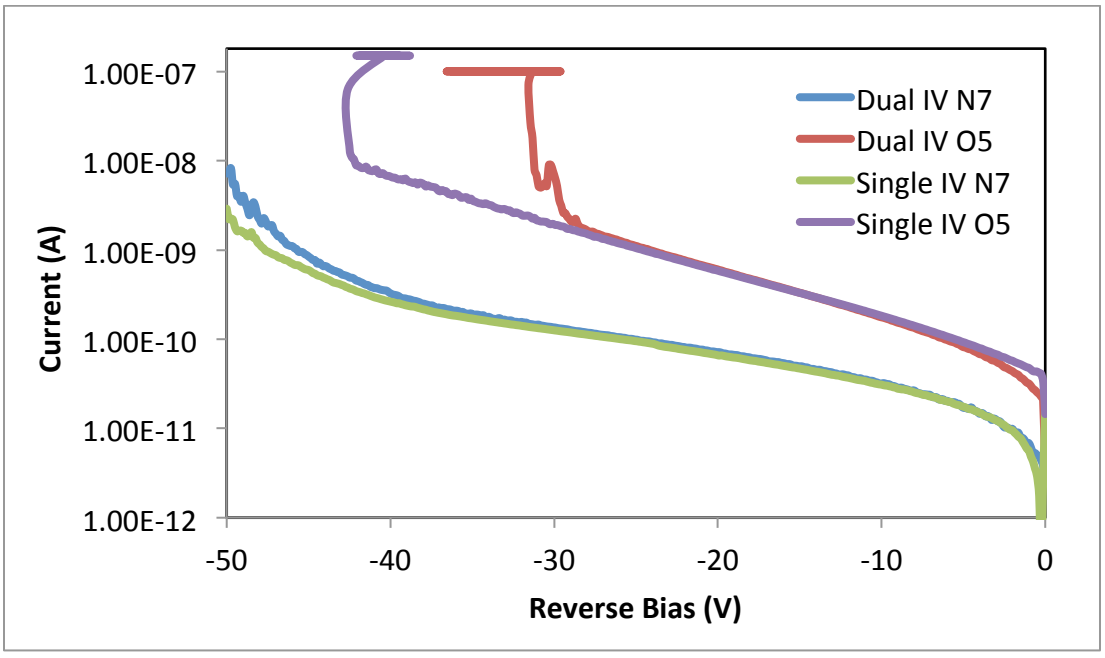

Figure 11. I-V curve of two diodes measured independently of one another, and simultaneously.

Spectra were first obtained using an ^{241}Am alpha source with both detectors biases to -25 V. Figure 12 shows the results of this experiment, with the high energy edge of both peaks quite close to one another. This is to be expected, as the depletion depth predicted in Figure 4 shows both diodes to have similar depletion depths at the same bias.

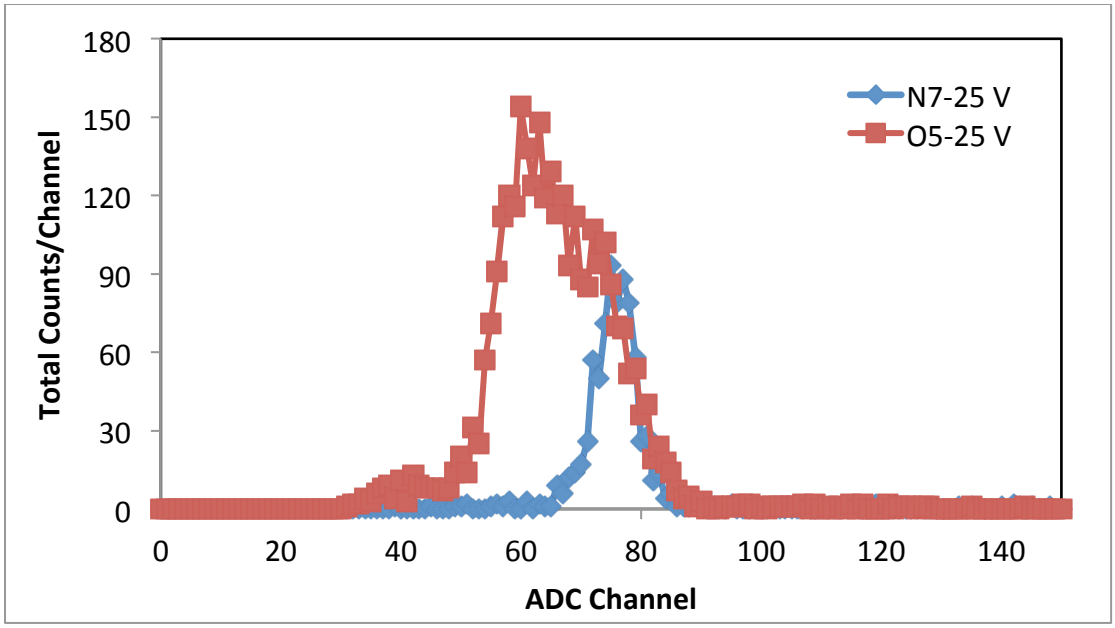

Figure 12. Alpha spectra obtained from diode N7 and O5 simultaneously biased to -25 V.

The experiment was repeated (Figure 13) with diode N7 biased to -50 V, as the leakage current in the diode at this voltage was still acceptably low. As expected, increasing the bias voltage in N7 shifted the peak centroid to a higher channel and broadened the spectrum due to the more collected charges and increased statistic errors.

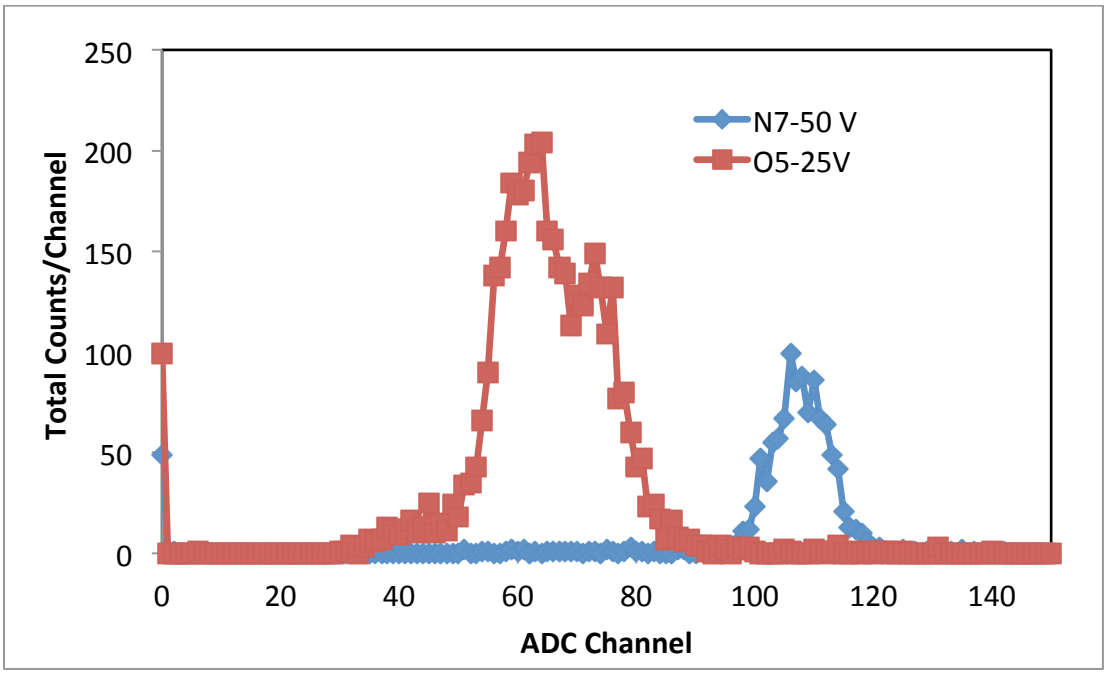

Figure 13. Alpha spectra obtained from diode N7 biased to -50 V and O5 biased to -25 V simultaneously.

The results of these experiments appear promising towards our goal of a gamma discriminating device. Future studies should include determining the reason for double peaks appearing in the spectra of several diodes, and creating a process to coat the detectors with a neutron sensitive material. Before the experiment on neutron converter coating, a numerical simulation is carried out to the device for understanding its charge collection process.

5. Device Simulation

5.1 Physical Models

In order to further understand the charge collection process in our GaN detectors, numerical simulations were performed using Sentaurus TCAD software package[5]. The basic parameters obtained from the previous experiments are listed in Table 3, which were incorporated into the simulation code. To minimize the calculation effort, a lateral size reduced 2D structure was employed by taking into account the area factor, the TCAD codes are attached in Appendix 1-5.

The incident energetic particle is a 5.48 MeV alpha particle (emitted by ^{241}Am source) and heavy ion model is employed. At time of 1×10^{-15} s, the particle incident upon the top Schottky contact perpendicularly, which is reverse biased at a certain voltage. The particle then deposit its energy to liberate e-h pairs along its track in GaN substrate, the linear transferred energy was calculated by SRIM and a simplified piecewise step function was used to approximate the deposited energy. The carriers generated vertically along the track are in a Gassian distribution. For carrier mobility, constant mobility and high field saturation models are chosen. For carrier recombination, radiative, Shockley-Read-Hall (SRH), and Auger recombination models are included. For carrier trapping, four hole traps and four electron traps are added with parameters taken from references [24, 25] shown in Table 4 and Table 5, respectively.

Table 3. Basic parameters of the GaN-based Schottky diode

Parameter	Value
Carrier concentration (cm^{-3})	1.68×10^{16} (CV)
Schottky barrier height (eV)	0.75 (IV)
Series resistance (Ohm)	10 (IV)

Table 4. Hole traps added in the TCAD simulation [24]

Name	Energy from valance band (eV)	Concentration (cm^{-3})	Capture cross section (cm^2)
H2	0.55	2.4E14	2.7E-12
H3	0.65	2.1E14	1.7E-14
H4	0.85	3.4E14	1.8E-13
H5	1.2	2.9E15	4.7E-14

Table 5. Table 5. Electron traps added in the TCAD simulation [25]

Name	Energy from Conduction band (eV)	Concentration (cm^{-3})	Capture cross section (cm^2)
L1	0.17	1.0E14	2.3E-17
L2	0.52	9.0E14	3.3E-16
L3	0.53	5.8E14	3.3E-17
L4	0.94	5.8E15	1.0E-16

Previous research confirmed that the collected charge mainly composed of two components from three different regions, i.e., the drift and diffusion carriers from depletion, funneling, and diffusion regions. Figure 14.Structure of the simulated GaN Schottky diode and the three regions for charge collection analysis. The purpose of this simulation was to understand the charge collection process, especially the CCE contributions of the carriers from the three different regions.

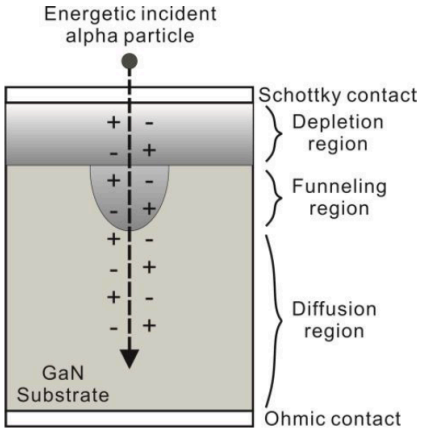

Figure 14.Structure of the simulated GaN Schottky diode and the three regions for charge collection analysis.

5.2 Comparison of Simulation and Experiment Results

With these physics models and parameters discussed before, Figure 15 compares the simulated and measured capacitance-voltage (C-V) and charge collection efficiency (CCE) characteristics of the device. The CCE is calculated by integrating the total transient current on Schottky side in a period of 10 ns. The well agreed simulation and experiment results indicate that all the major physics models are correctly incorporated in our model.

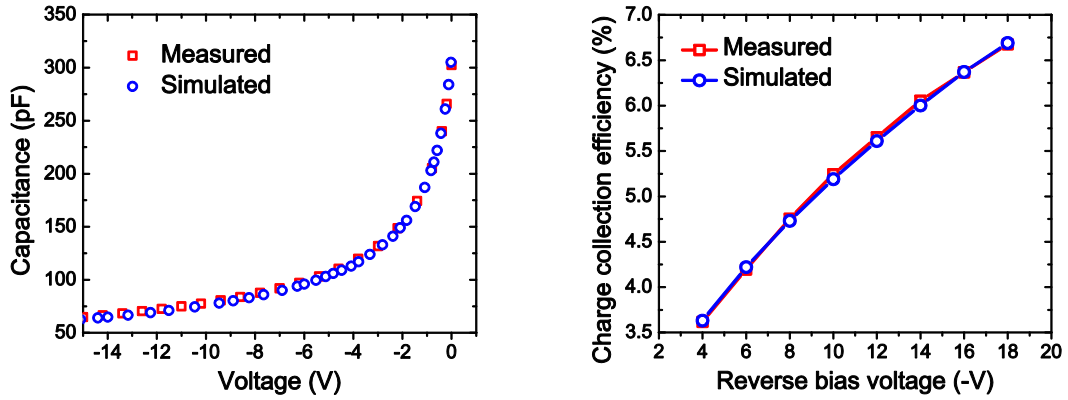

Figure 15. Simulated and measured results, left: capacitance-voltage; and right: charge collection efficiency.

5.3 Transient Current Analysis

Figure 16 shows the total transient current of the device when reverse biased at different voltages. The results indicate that, higher bias voltage generate higher transient current with faster collection time, which can be explained by the increased collected charge (the width of the depletion region is increased) and the increased carriers' velocities (the electric field within the semiconductor region is increased), respectively.

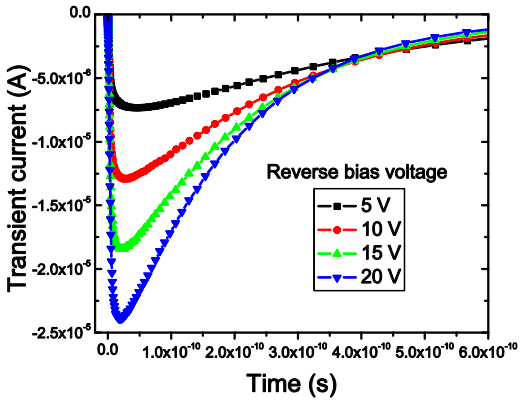

Figure 16. Simulated total transient current at different reverse bias voltages on the Schottky side.

Figure 17 shows the induced transient currents of different components when the diode is reversed biased at -20 V, from which it can be concluded that: 1) On Schottky side, the total transient current is the evolution of both holes and electrons; however on Ohmic side, the total transient current is solely composed of electrons; 2) On Schottky side, the hole component goes through a fast transient; and 3) the total transient current is mainly composed of a fast ramp and a slow decay components. All of these characteristics are well explained by the high built-in electric field, the thin depletion region, and the lifetimes and motilities of the carriers. For instance, even the mobility of the hole is smaller (~ 10 $cm^2/V{\cdot}s$), they can be collected in a very short time due to the thin depletion region (1 micrometer). In addition, holes generated in the bulk region cannot be collected due to their short lifetime (~1 ns), thus only the holes created in the depletion region contribute to the collected charge. That is why the holes create a superfast transient current without a decay tail. On the contrary, electrons generated in the depletion region and bulk region are both contribute to the collected charge, and electrons in the bulk region (low electric field) move much slower than the ones generated in the depletion region (high built-in electric field), all of which make the

electron transient current characterized by a fast drift followed by a slow diffusion component.

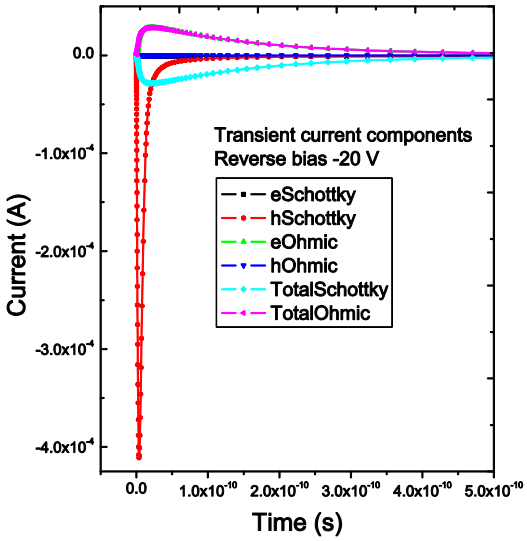

Figure 17. Simulated different components of the transient current created by a 5.48 MeV alpha particle at a reverse bias of -20 V.

When the diode is reverse biased at -5 V, Figure 18 and Figure 19 further visualized the electron and hole current density near the Schottky contact at different transient times induced by the 5.48 MeV alpha particle, from which the evolution of the funneling region can be clearly seen.

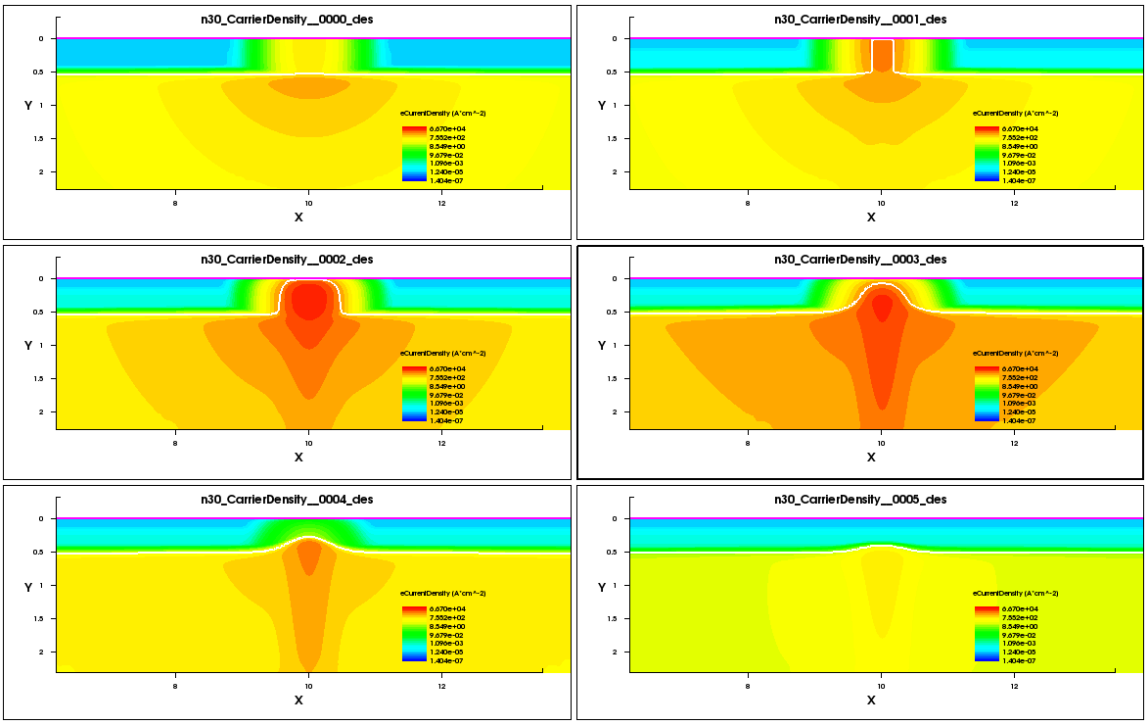

Figure 18. Simulated electron current densities at times of 1e-14, 1e-13, 1e-12, 5.2e-12, 1e-11, and 1e-10 second, the units for both x- and y-axes are micrometer.

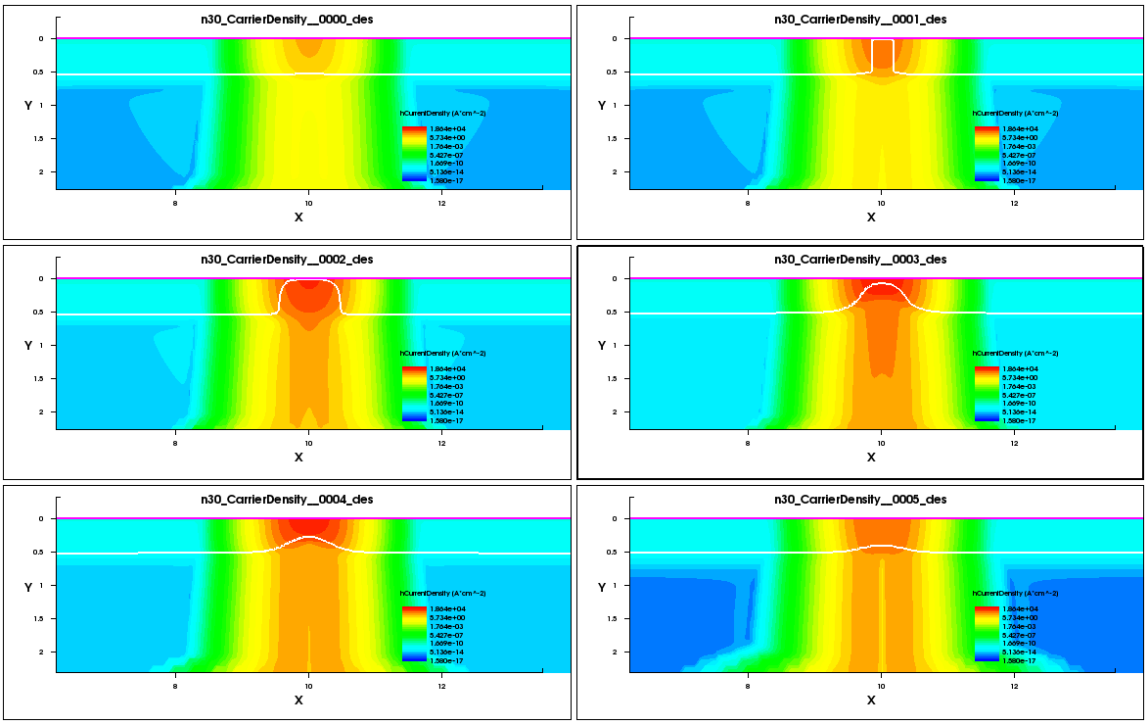

Figure 19. Simulated hole current densities at times of 1e-14, 1e-13, 1e-12, 5.2e-12, 1e-11, and 1e-10 second, the units for both x- and y-axes are micrometer.

5.4 Charge Collection Efficiency

Further simulations indicate that the width of the funneling region is independent of the applied voltage, i.e., about 1 micrometer for all bias conditions when the hole transient current reaches its maximum. Thus we divided the GaN substrate into three regions: depletion region (depending on the applied voltage), funneling region (with a width of 1 micrometer), and diffusion region (all the remaining GaN substrate). By sending the alpha particle into different regions and subtracting the corresponding collected charges, the charge collection efficiencies contributed by different components can be derived (see Figure 20). The result indicates that for Schottky diode detectors fabricated on moderately doped semiconductors (~10^{16} cm^{-3} in our case), the drift carriers in the depletion region is still the major component of the collected charges.

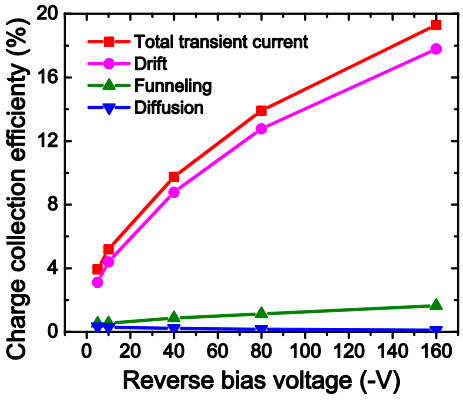

Figure 20. Contributions of different transient current components to the charge collection efficiency.

6. Gamma-ray Discrimination

6.1 Gamma-ray Discrimination Scheme

Although the small volume and low Z number of a thin-film semiconductor detector (e.g., Si) make it relatively insensitive to external gamma rays, those low-energy external gamma rays that fall within the ICE energy range could lead to false positive neutron detection. One such application where this could present an issue is in special nuclear material (SNM) detection, which typically occurs in environments that are "neutron signal starved", but "gamma signal abundant" [26]. To mitigate the likelihood of a false detection due to gamma rays, a twin-detector scheme is proposed using Gd as a neutron converter, and two detectors to identify and rejecting external gamma rays, as shown in Figure 21. Rejection is achieved by introducing a layer of Gd foil and another layer of an electron separator material (polyethylene) into the composite detector scheme. Detector 1 is placed in direct contact with a Gd foil, allowing the detection of ICEs, as well as gamma rays produced by neutron absorption in Gd. A second detector is placed on the rear of the Gd layer, but uses a polyethylene layer of appropriate thickness to stop all Gd generated ICEs and Auger electrons from reaching detector 2. In this configuration, detector 2 is sensitive only to gamma rays. Hence, detector 1 generates a combined signal induced by both neutrons and gamma rays, whereas detector 2 produces a signal induced only by gamma rays. Subtracting the two detector signals would yield a net signal induced solely by neutrons.

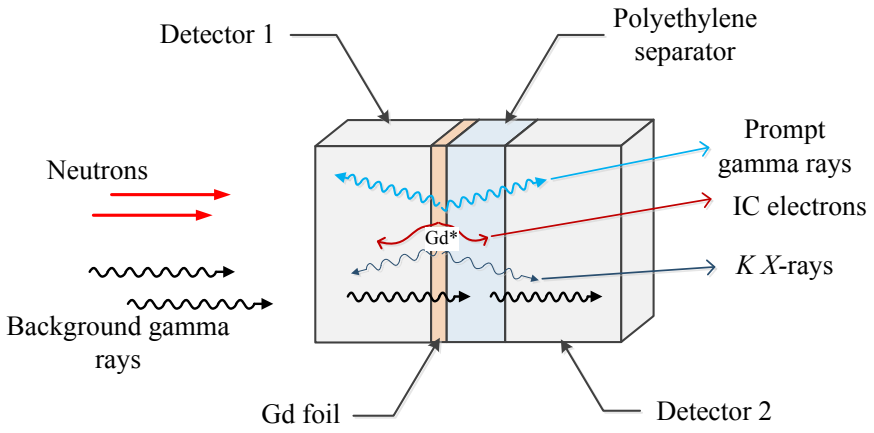

Figure 21. Gamma ray rejection scheme with two semiconductor detectors, a Gd layer and a polyethylene layer.

Some limitations of the proposed method were also identified during a preliminary investigation and are presented below.

1) The direct interaction of external gamma rays with detectors 1&2 is supposed to generate identical response in the detectors. In addition, *K-X* rays emitted from gamma ray activation of Gd induce identical response in the detectors. Subtraction of the two detector signals effectively cancels out the identical gamma ray component in the resultant signal. However, electrons emitted due to photoelectric absorption in Gd penetrate detector 1 but are blocked by the polyethylene separator from reaching detector 2. Thus, a residual gamma ray component due to photoelectrons still exists in the resultant signal after subtraction.

2) Unlike the case in PSD, event by event separation of neutrons and gamma rays is not achieved with the proposed method.

6.2 Experiment Setup

The proposed gamma ray rejection scheme is heavily dependent on the detection of ICE signal for registering neutron events. Although a large number of prompt gamma rays in addition to characteristic x-rays are released in Gd neutron reaction, the associated component of the neutron signal is effectively cancelled out when subtracting the two detector signals. In order to validate our assumption, ICE detections was first done on Si based detectors, and the experiment setup is schematic illustrated in Figure 22. The whole setup is incorporated into the OSU research reactor, which can provide a neutron radiation environment with high gamma-ray dose.

In this experiment, a thin Gd foil (1.25 cm × 1.25 cm × 0.0025 cm) was mounted on the sample holder inside the high-vacuum chamber. The multidetector setup provided an opportunity to acquire multiple spectra during one experiment. Therefore, two of the eight Si charged particle detectors were covered with 350 μm thick polyethylene caps to shield them from the ICEs, while the remaining six detectors were left unshielded. A background measurement was also performed at the same instrument settings by removing the Gd foil from the chamber.

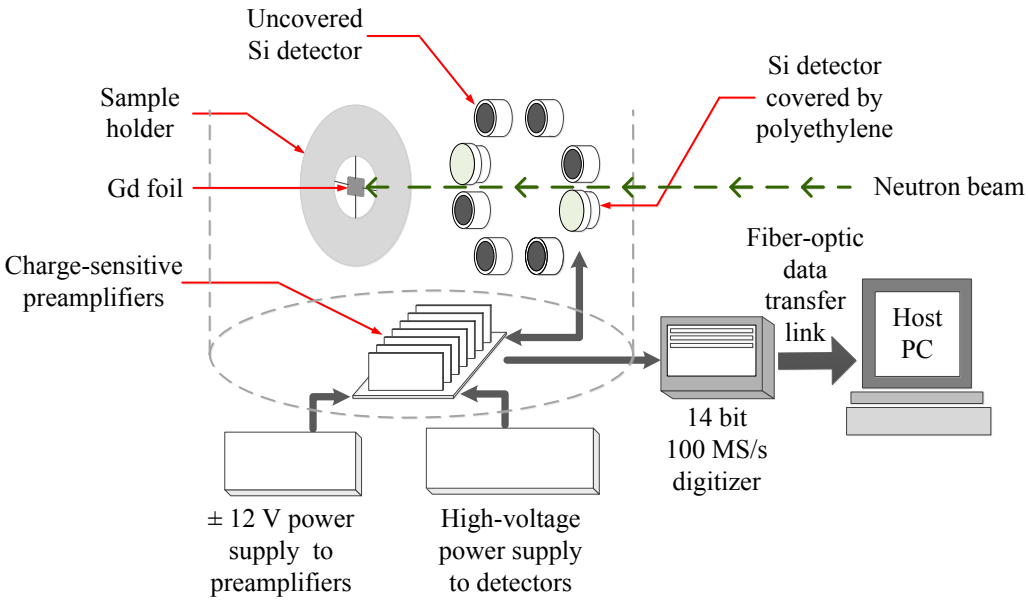

Figure 22. Schematic illustration of the experimental setup and the DAQ electronics used in the ICE measurements.

6.3 Performance of Gd Covered Si Detector at Low Reactor Power

For the first experiment, the reactor operated at 5 kW_{th} and delivered a thermal equivalent neutron flux of about 9.6×10^4 $cm^{-2} \cdot s^{-1}$ and a gamma dose rate of about 27 $mRad \cdot hr^{-1}$ at the sample location. A lower level threshold of 23.3 keV was set on the detector pulses. The measured results showed that the energy spectra of the six uncovered (*i.e.*, unshielded from ICEs) Si detectors were identical, and the energy spectra of the two covered (*i.e.*, shielded from ICEs) Si detectors were also identical to each other.

Energy spectra representative of the two sets detectors obtained after background subtraction are illustrated in Figure 23. A highly intense and broad energy peak centered at ~71 keV is clearly seen from the bare detectors; in addition, two much less intense peaks at 131 keV and 173 keV are also visible. The origin of the 71 keV peak is due to the combined energy deposition of 29-88 keV ICEs and characteristic x-rays in the detector. The peak broadening is attributed in part to the limited energy resolution of the

detector, but more to the fact that ICEs lose energy when escaping the Gd foil before reaching the Si detector. On the other hand, the energy spectrum from the covered detectors indicates that the 350 μm thick polyethylene layer completely blocked the ICEs while still permitting gamma/x-rays to pass. An MCNP5 simulation confirmed that the 350 μm thick polyethylene cap used in this study can absorb gamma rays only up to ~15 keV.

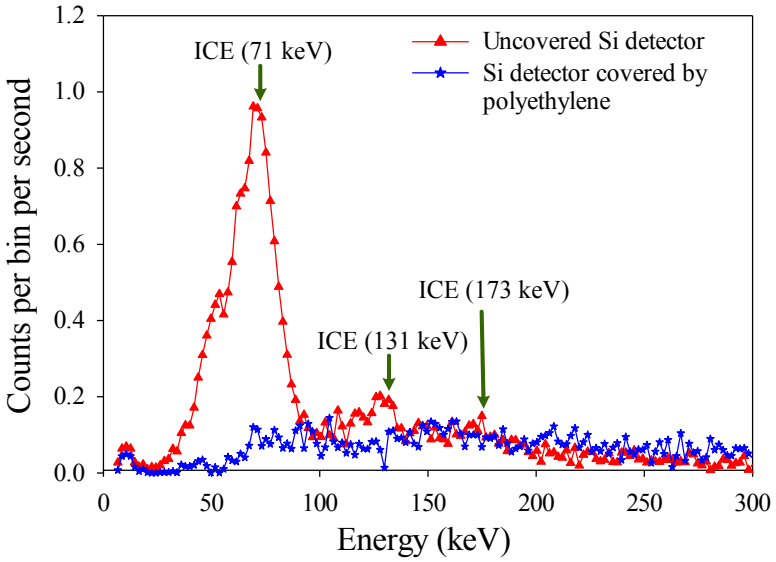

Figure 23. ICE energy spectrum measured using Si detectors during neutron activation of a thin Gd foil.

The experimental results indicate that the energy spectra from the bare detectors is attributed to mixed ICE and gamma ray response, whereas that from the polyethylene covered detectors is due only to gamma/x-rays. Thus, the neutron signal may be effectively separated from the gamma ray background by using the proposed gamma-ray rejection scheme of Figure 21. The results also validate the hypothesis that the prompt gamma rays from Gd^{*} are almost transparent to a small volume semiconductor detector (e.g., Si), while the ICEs constitute the principal neutron signal in such a detector.

6.4 Performance of Gd Covered Si Detector at High Reactor Power

The Gd ICE measurement was repeated at a higher neutron flux by increasing the reactor power to 250 kW_{th}. The thermal equivalent neutron flux and the gamma dose rate were observed as 4.8×10^6 $cm^{-2} \cdot s^{-1}$ and 1.35 $Rad \cdot hr^{-1}$ respectively. A lower level threshold of 20.1 keV was set on the detector pulses. The energy spectra acquired from the uncovered and covered detectors and the experimental geometry in inset are shown in Figure 24. As expected, due to higher neutron flux, the uncovered detector spectrum indicated much greater energy resolution with the three characteristic ICE peaks clearly resolved. An interesting feature is the small peak at ~48 keV on the slope of the main peak, which is due to the characteristic x-rays of Gd activated by neutrons as well as gamma rays. This peak is clearly identified in the energy spectrum of covered detector due to the separation of ICEs.

The results also indicate that the separation of gamma rays can be effective even at a much higher gamma dose rate. However, a fair judgment on the efficacy of the discrimination technique may only be possible with a measurement in a gamma abundant and neutron deficient radiation environment.

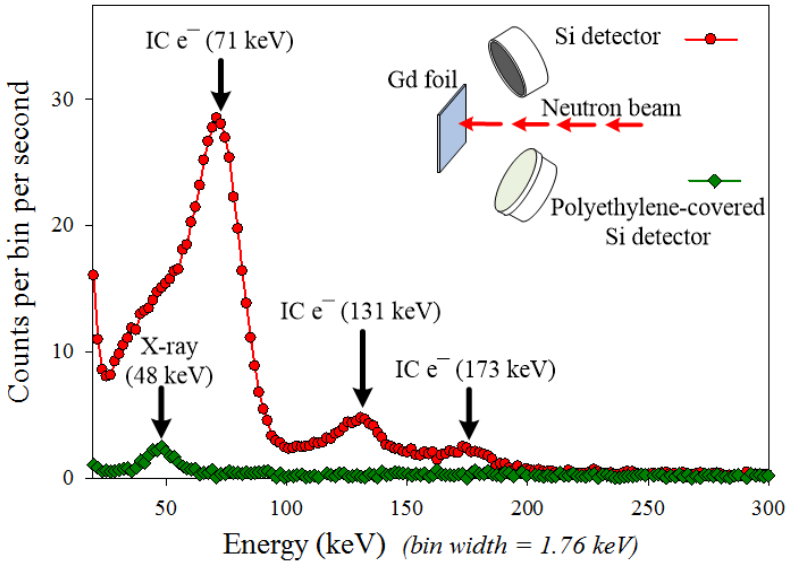

Figure 24. ICE energy spectrum measured using Si detectors during neutron activation of a thin Gd foil at a higher neutron flux and gamma dose rate.

6.5 Performance of LiF Thin Film Covered GaN Twin-detector

The feasibility of a GaN based, gamma discriminating neutron detector was tested at the OSU research reactor using a ^{6}LiF:ZnS thin film as the neutron conversion material. Two detectors fabricated on the same GaN wafer were used to simultaneously detect neutron induced reactions in the ^{6}LiF converter and gamma interactions. Both detectors were first used to observe alpha particle emissions from ^{239}Pu, verifying that both detectors were operating properly, as shown in Figure 25. One of the detectors (O7) displayed a centroid in a higher channel than the second detector (O5), due to the fact that detector O7 has a thicker depletion region and collects more electron-hole pairs generated by the incident alpha particles.

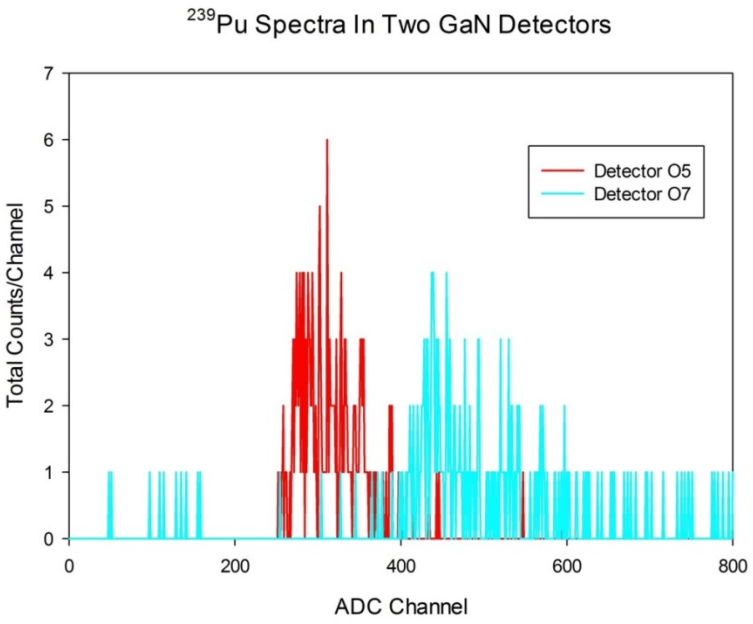

Figure 25. Alpha particle spectrum from 239Pu in GaN detectors O7 and O5 to verify both detectors were working properly.

The detectors were then covered by two Teflon apertures and a thin film (0.3 mm) ^{6}LiF:ZnS scintillation screen. One of the two apertures supported the scintillation screen, while the second completely covered one of the detectors (O5), leaving the second detector with an unobstructed path to the LiF:ZnS film (Figure 26).

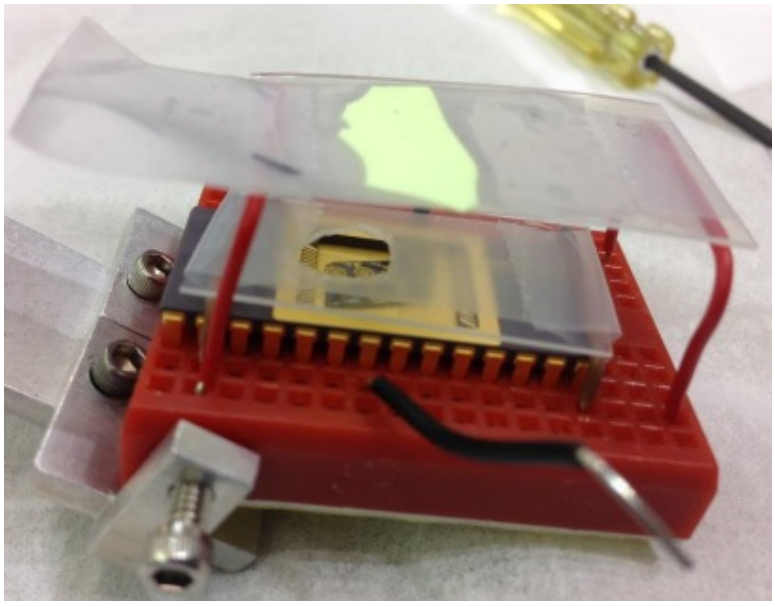

Figure 26. GaN detectors mounted in dual inline package with two Teflon apertures. 6LiF:ZnS converter film is the light green material on the upper aperture. The lower Teflon aperture leaves detector O7 exposed to the film, and completely covers detector O5.

The apparatus depicted in Figure 26 was then mounted in a vacuum chamber at the OSU Research Reactor neutron beam facility. Electrical connections were made to the GaN detectors and connected to a charge sensitive preamp. Output from the preamp was connected to a 14-bit digitizer with a trapezoidal filter, and then to a PC. The detectors were placed directly in the 3 cm neutron beam with the reactor operating at 250 kW thermal power (Figure 27).

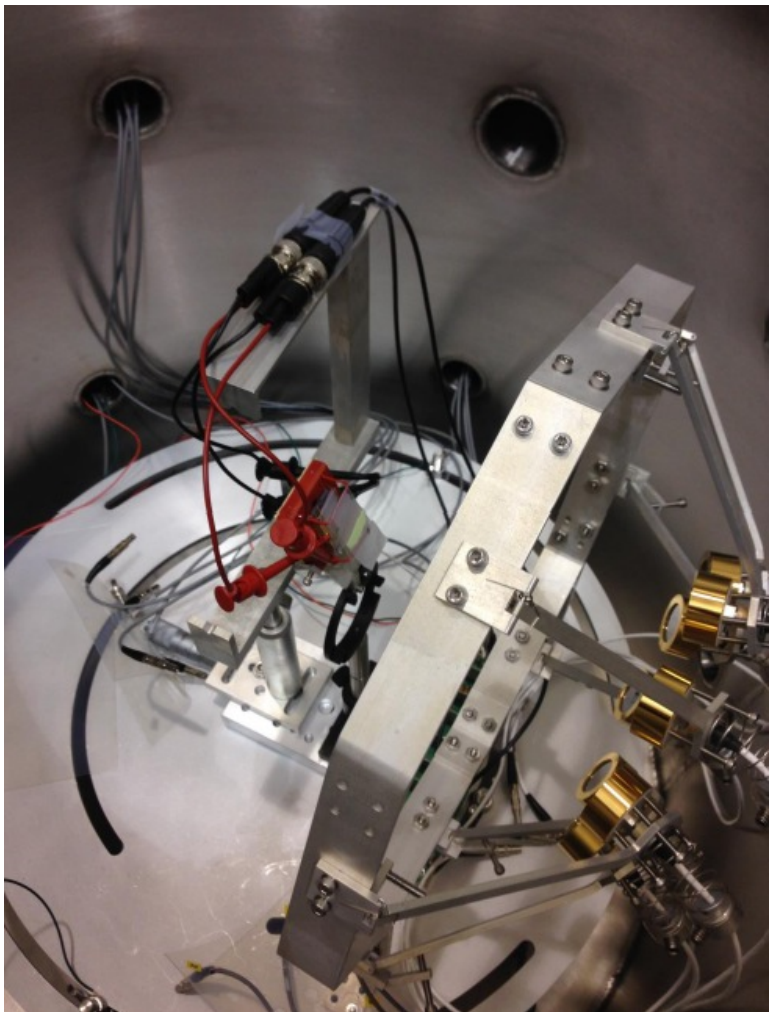

Figure 27. Detector setup in vacuum chamber at OSU research reactor neutron beam facility.

Results of the experiment are depicted in Figure 28. The two charged particles emitted from ^{6}Li, ^{3}H at 2727 keV and ^{4}He at 2055 keV, were clearly discernable in the spectrum collected by the uncovered detector. However, since the depletion depth of the detector was 1.6 μm, much less than the range of these particles in GaN, only a fraction of the particles' initial energy was deposited in the active region of the detector. Since the stopping power of the ^{4}He is greater than the stopping power of ^{3}H, ^{4}He deposited more energy in the depletion region than ^{3}H. By performing a SRIM calculation, it was determined that 771 keV was deposited by the ^{4}He particle in the depletion layer, and 135 keV was deposited by the ^{3}H. These values were then used to perform an energy calibration on the peaks in the uncovered detector. The covered detector did not exhibit a response to charged particles, which is expected, but did have a significant low energy signal below 50 keV, likely due to gamma rays in the neutron beam.

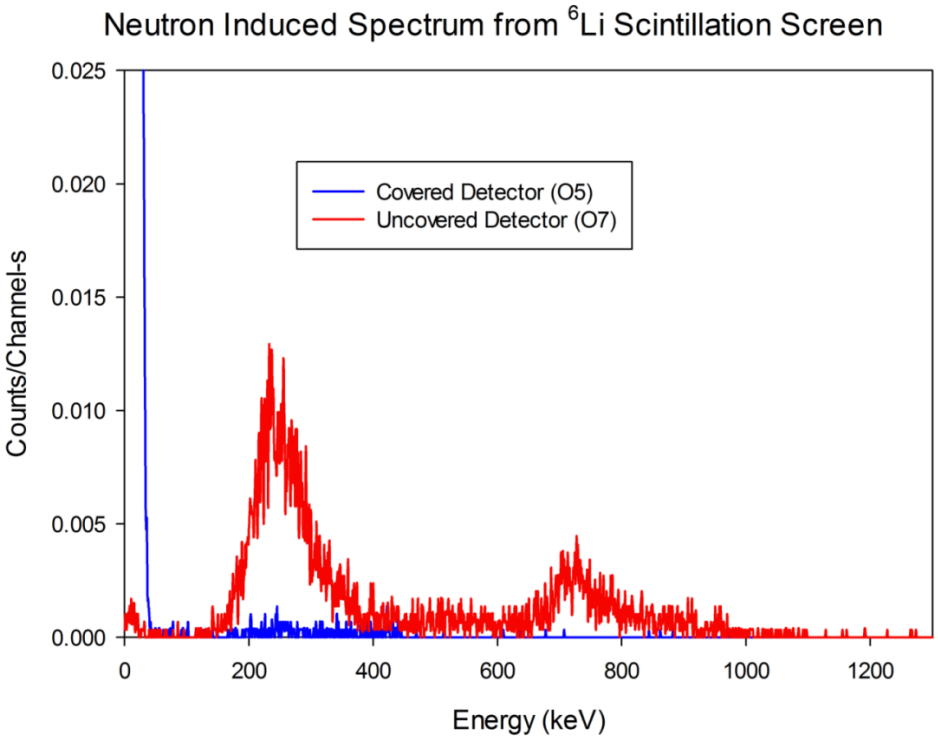

Figure 28. Observed spectrum from the uncovered detector (red) and covered detector (blue) due to charged particle emissions following ^{6}Li neutron capture. Energy calibration was performed using SRIM, and fitting Gaussian distributions to two peaks in the uncovered detector.

7. Conclusions

The goals accomplished and achievement made during the past two-years' research are:

1) Sandwiched structure Schottky diode radiation sensor was successfully fabricated on n-type freestanding GaN, presenting both alpha and neutron response;
2) By employing a special growth GaN wafer, the electric properties of the fabricated detector was improved, the level of leakage current is comparable with commercially available Si detector and is capable of producing high quality spectrometry. In addition to alpha particle, the detector also showed beta particle response;

3) Numerical simulations using Sentaurus TCAD package was performed to understand the fundamental material and device properties at picosecond scale, the charge collection process and transit properties within the device were studied;
4) A twin-detector scheme was designed and the concept for gamma-ray discrimination was validated by using Si detectors at both low and high neutron flux;
5) The GaN twin-detector structure was fabricated and evaluated by using alpha particle and ^{6}Li, its capability for neutron detection was validated.

Two-years' research has brought the TRL of the proposed technology to 3 or 4. With a complete set of understanding for both GaN materials and devices that are provided with this study, it is clear that GaN is capable of serving as a base material for neutron detection. The challenge is obtaining the higher purity materials to form thicker depletion regions for full spectrum measurement. One patent application is filed. Three graduate students have dedicated to this project, and their research efforts culminated the production of two MS thesis, one PhD thesis, seven journal papers, and eight conference proceedings.

PhD Dissertation:

1) "Gamma Rays Rejection in a Gadolinium based Semiconductor Neutron Detector", Praneeth Kandlakunta, 2013

MS Thesis:

1) "A Proof-of-Principle Investigation for a Neutron-Gamma Discrimination Technique in a Semiconductor Neutron Detector", Praneeth Kandlakunta, 2012
2) "Evaluation of GaN as a Radiation Detection Material ", Jinghui Wang, 2012

Journal Articles:

1) P. Kandlakunta, L.R. Cao, Neutron Conversion Efficiency and Gamma Interference with Using Gadolinium. Journal of Radioanalytical and Nuclear Chemistry (accepted).
2) Mulligan, P., J.H. Wang, and L. Cao, Evaluation of freestanding GaN as an alpha and neutron detector. Nuclear Instruments & Methods in Physics Research Section a-Accelerators Spectrometers Detectors and Associated Equipment, 2013. 719: p. 13-16.
3) Kandlakunta, P. and L. Cao, Gamma-ray rejection, or detection, with gadolinium as a converter. Radiation Protection Dosimetry, 2012. 151(3): p. 586-590.
4) Kandlakunta, P., L.R. Cao, and P. Mulligan, Measurement of internal conversion electrons from Gd neutron capture. Nuclear Instruments & Methods in Physics Research Section a-Accelerators Spectrometers Detectors and Associated Equipment, 2013. 705: p. 36-41.
5) Jie Qiu, E.K., Lei R. Cao, Leonard J. Brillson, The Evaluation of GaN for Neutron Detector with Cathodoluminescence Spectroscopy. Transactions of American Nuclear Society, 2012. 107: p. 357-359.
6) J. Ralston, P.K., L. Cao, Electron Emission Following ^{157}Gd Neutron Capture. Transaction of American Nuclear Society, 2012. 106: p. 313-315.
7) Padhraic Mulligan, J.Q., Jinghui Wang, Lei R. Cao, Study of Gallium Nitride for High-Level Neutron Field Measurement. IEEE Transactions on Nuclear Science (Accepted). 2013.

Conference Proceedings:

1) Lei R. Cao, Praneeth Kandlakunta, "Measure Internal Conversion Electron Spectrum of Gadolinium Neutron Capture Using Neutron Beam." In: Transactions of American Nuclear Society, (Aug 2013) 108, p.267 - 269.
2) Praneeth Kandlakunta, Padhraic Mulligan, Danyal Turkoglu, Lei Cao, "A Neutron Flux Monitor for a Reactor Neutron Beam Facility", IEEE Nuclear Science Symposium and Medical Imaging Conference (NSS/MIC) Record, 2012, Anaheim, CA, USA.

3) J. Ralston, P. Kandlakunta, L. Cao, "Electron Emission Following ^{157}Gd Neutron Capture." American Nuclear Society Annual Meeting 2012, Chicago, IL, USA
4) Praneeth Kandlakunta, Lei Cao, "A Neutron Detector with Gamma Discrimination." In: Transactions of the American Nuclear Society. Vol. 105. Washington, D.C., USA. (2011):335-336.
5) Jinghui Wang, Praneeth Kandlakunta, Thomas F. Kent, John Carlin, Daniel R. Hoy, Roberto C. Myers, Lei Cao, "A Gadolinium Doped Superlattice GaN Schottky Diode for Neutron Detection." In: Transactions of the American Nuclear Society. Vol. 104. Hollywood, FL, USA (2011): 207-209.
6) Mulligan, P., "Development of an Alpha Detector on Freestanding n-GaN. Presented at 2013 Chemical Biology Radiation Nuclear Symposium, Peers within Field. Air Force Institute of Technology, Wright-Patterson AFB, Fairborn, OH, United States, April 3, 2013.
7) Mulligan, P., "Fabrication and Characterization of a Freestanding n-type GaN Radiation Detector." Presented at 2013 American Nuclear Society Student Conference, Boston, MA, United States, April 5, 2013.
8) Wang, J., "Developing a Radiation Detector on Freestanding n-GaN." Presented at American Nuclear Society 2013 Annual Meeting, Atlanta, GA, United States, June, 2013.

References

1. http://www.ammono.com/.

2. Jinghui Wang, P.K., et al., *A Gadolinium Doped Superlattice GaN Schottky Diode for Neutron Detection.* Transactions of the American Nuclear Society, Hollywood, Florida, June 2011. 104.

3. http://www.kymatech.com/.

4. Mulligan, P., J.H. Wang, and L. Cao, *Evaluation of freestanding GaN as an alpha and neutron detector.* Nuclear Instruments & Methods in Physics Research Section a-Accelerators Spectrometers Detectors and Associated Equipment, 2013. 719: p. 13-16.

5. http://www.synopsys.com.

6. Mulligan, P., *Development of a Multi-detector Digital Neutron Depth Profiling Instrument at the Ohio State University.* Thesis, The Ohio State Univerity, 2012.

7. Wang, J., *Evaluation of GaN as a Radiation Detection Material.* Thesis,The Ohio State University, 2012.

8. Kandlakunta, P., *Gamma Rays Rejection in a Gadolinium based Semiconductor Neutron Detector.* Thesis,The Ohio State Univeristy, 2013.

9. P. Kandlakunta, L.R.C., *Neutron Conversion Efficiency and Gamma Interference with Using Gadolinium.* Journal of Radioanalytical and Nuclear Chemistry (accepted). 2013.

10. Kandlakunta, P. and L. Cao, *Gamma-ray rejection, or detection, with gadolinium as a converter.* Radiation Protection Dosimetry, 2012. 151(3): p. 586-590.

11. Kandlakunta, P., L.R. Cao, and P. Mulligan, *Measurement of internal conversion electrons from Gd neutron capture.* Nuclear Instruments & Methods in Physics Research Section a-Accelerators Spectrometers Detectors and Associated Equipment, 2013. 705: p. 36-41.

12. Jie Qiu, E.K., Lei R. Cao, Leonard J. Brillson, *The Evaluation of GaN for Neutron Detector with Cathodoluminescence Spectroscopy.* Transactions of American Nuclear Society, 2012. 107: p. 357-359.

13. J. Ralston, P.K., L. Cao, *Electron Emission Following 157Gd Neutron Capture.* Transaction of American Nuclear Society, 2012. 106: p. 313-315.

14. Padhraic Mulligan, J.Q., Jinghui Wang, Lei R. Cao, *Study of Gallium Nitride for High-Level Neutron Field Measurement.* IEEE Transactions on Nuclear Science (Accepted). 2013.

15. Jinghui Wang, P.M., Lei R. Cao, *A Survey of Using GaN for Ionizing Radiation Detection.* 2013.

16. Jinghui Wang, P.M., Lei Cao, *Understanding charge collection process in a GaN-based Schottky diode radiation detector by TCAD modeling.* 2013.

17. Kandlakunta, P., *Measure Internal Conversion Electron Spectrum of Gadolinium Neutron Capture Using Neutron Beam.* Presented at American Nuclear Society 2013 Annual Meeting, Atlanta, GA, United States, June 2013.

18. Praneeth Kandlakunta, P.M., Danyal Turkoglu, Lei Cao, *A Neutron Flux Monitor for a Reactor Neutron Beam Facility.* IEEE Nuclear Science Symposium and Medical Imaging Conference (NSS/MIC) Record, 2012 Anaheim, CA, USA.

19. Praneeth Kandlakunta, L.C., *A Neutron Detector with Gamma Discrimination.* Transactions of the American Nuclear Society, 2011, Washington, D.C., USA. 105: p. 335-336.

20. Mulligan, P., *Development of an Alpha Detector on Freestanding n-GaN.* Presented at 2013 Chemical Biology Radiation Nuclear Symposium, Peers within Field. Air Force Institute of Technology, Wright-Patterson AFB, Fairborn, OH, United States, April 3, 2013.

21. Mulligan, P., *Fabrication and Characterization of a Freestanding n-type GaN Radiation Detector.* Presented at 2013 American Nuclear Society Student Conference, Boston, MA, United States, April 5, 2013.

22. Wang, J., *Developing a Radiation Detector on Freestanding n-GaN.* Presented at American Nuclear Society 2013 Annual Meeting, Atlanta, GA, United States, June, 2013.

23. Lee, I.H., et al., *Electrical properties and radiation detector performance of free-standing bulk n-GaN.* Journal of Vacuum Science & Technology B, 2012. 30(2).

24. Polyakov, A.Y., et al., *Comparison of hole traps in n-GaN grown by hydride vapor phase epitaxy, metal organic chemical vapor deposition, and epitaxial lateral overgrowth.* Journal of Applied Physics, 2011. 109(12).

25. Py, M.A., et al., *Characterization of deep levels in n-GaN by combined capacitance transient techniques.* Physica Status Solidi a-Applications and Materials Science, 2005. 202(4): p. 572-577.

26. Kouzes, R.T., et al., *Neutron detection alternatives to He-3 for national security applications.* Nuclear Instruments & Methods in Physics Research Section a-Accelerators Spectrometers Detectors and Associated Equipment, 2010. 623(3): p. 1035-1045.

Appendix 1: TCAD code for structure construction

```
; Sandwich structure Schottky diode based on Kyma freestanding n-type GaN
; Write by Jinghui Wang, 04-05-2013
; ==================== Outer Boundary Creation ========================
;---Define dimensions
(define wsub 20)
(define tsub 430)
(define tepi 20)
(define tepisub 450)

(define sleft 0)
(define sright 20)

;---GaN Regions
(sdegeo:create-rectangle  (position 0.0 0.0 0.0) (position wsub tepisub 0.0) "GaN" "EpiSubRegion" )


; ==================== Contact Definition Placement  ========================
(sdegeo:define-contact-set "top_schottky" 4.0 (color:rgb 1.0 0.0 0.0) "##")
(sdegeo:define-contact-set "bot_ohmic" 4.0 (color:rgb 0.0 1.0 0.0) "//")

(sdegeo:insert-vertex (position sleft 0.0 0.0))
(sdegeo:insert-vertex (position sright 0.0 0.0))

(sdegeo:define-2d-contact (find-edge-id (position  5 0.0 0.0)) "top_schottky")
(sdegeo:define-2d-contact (find-edge-id (position  5 tepisub 0.0)) "bot_ohmic")


; ==================== Constant and Analytical Profiles ========================
;---Definitions
(sdedr:define-constant-profile "Sub_Dop_Defn" "PhosphorusActiveConcentration" 1.68e+16)

;---Windows
(sdedr:define-refeval-window "Sub_Win"  "Rectangle"  (position 0 0 0) (position wsub tepisub 0.0))

;---Placement
(sdedr:define-constant-profile-placement "Sub_Place" "Sub_Dop_Defn" "Sub_Win")


; ==================== Refinements  ========================
;---Definitions
(sdedr:define-refinement-size "Sub_Ref_Defn"   4.0 4.0 0.0   0.8 0.8 0.0 )
(sdedr:define-refinement-size "Epi_Ref_Defn"   1.0 0.4 0.0   0.2 0.1 0.0 )


;---Windows
(sdedr:define-refinement-window  "Sub_Win" "Rectangle"  (position 0.0 0.0 0.0) (position wsub tepisub
0.0) )
(sdedr:define-refinement-window  "Epi_Win"  "Rectangle" (position 0.0 0.0 0.0) (position wsub tepi 0.0) )


;---Placement
(sdedr:define-refinement-placement "Sub_Ref_Place" "Sub_Ref_Defn" "Sub_Win" )
(sdedr:define-refinement-placement "Epi_Ref_Place" "Epi_Ref_Defn" "Epi_Win" )
```

```
; JC: Add mesh refinement near Schottky electrode for proper construction of NLM in SDevice
(sedr:define-refeval-window "RefWin.Schottky" "Rectangle"  (position sleft 0.0 0) (position sright 0.025
0))
(sedr:define-refinement-size "RefDef.Schottky" 0.05 0.005 0 0.01 0.001 0 )
(sedr:define-refinement-function "RefDef.Schottky" "MaxLenInt" "GaN" "All" 0.001 4)
(sedr:define-refinement-placement "RefPlace.Schottky" "RefDef.Schottky" "RefWin.Schottky" )

; JC: Add mesh refinement to cover depletion region at most negative bias
(sedr:define-refeval-window "RefWin.Depletion" "Rectangle"  (position (- sleft 0) 0.0 0) (position (+
sright 0) 2 0))
(sedr:define-refinement-size "RefDef.Depletion" 0.05 0.05 0 0.05 0.05 0 )
(sedr:define-refinement-placement "RefPlace.Depletion" "RefDef.Depletion" "RefWin.Depletion" )

; WJH:Add mesh refinement for incident ion region
#(sedr:define-refeval-window "RefWin.Iontrack" "Rectangle"  (position 47 0.0 0) (position 53 25 0))
#(sedr:define-refinement-size "RefDef.Iontrack" 0.02 0.02 0 0.01 0.01 0 )
#(sedr:define-refinement-placement "RefPlace.Iontrack" "RefDef.Iontrack" "RefWin.Iontrack" )



;---Resolve the junction
#(sdeaxisaligned:set-parameters "yCuts"   (list 9.99 10.0 10.01))
;-----------------------------------------------------------------------
; Build Mesh
(sde:build-mesh "snmesh" " " "n@node@_msh")
```

Appendix 2: TCAD Code for I-V Simulation

*****IV simulation-sdevice code****

```
File {
        Grid= "@tdr@"
        Plot= "@tdrdat@"
        Current= "@plot@"
        Output= "@log@"
        Parameter= "@parameter@"
}

Electrode {
        { Name="top_schottky" Schottky Barrier= 0.75 Voltage= 0.0 }
        { Name="bot_ohmic" Voltage= 0.0 Resist=10 }
}

Physics {
        Temperature= 300
        AreaFactor=15700
        Recombination (
        Radiative
        SRH(
          DopingDependence
          TempDependence
          # ElectricField(Lifetime=Hurkx DensityCorrection=None)
          )
        Auger
        #Avalanche (vanOverstraetendeMan)
        )

        eBarrierTunneling "NLM"

        Mobility (
          ConstantMobility
          #DopingDependence(Masetti)
          HighFieldSaturation
    )

        EffectiveIntrinsicDensity ( OldSlotboom NoFermi )
}

Physics (Region= "EpiSubRegion") {
        Optics (OpticalGeneration (SetConstant (Value= 1e16)))
}

Plot {
        eDensity hDensity
        eMobility hMobility
        eVelocity hVelocity
        eCurrent hCurrent
        eQuasiFermi hQuasiFermi
        egradQuasiFermi hgradQuasiFermi
        Doping
        DonorConcentration
        AcceptorConcentration
        ElectricField
        Potential
```

```
        SpaceCharge
        ConductionBandEnergy
        ValenceBandEnergy
        BandGap
        RadiativeRecombination
        SRH
        SRHRecombination
        Auger
        AvalancheGeneration
        eAvalanche hAvalanche
        #OpticalGeneration
        #OpticalIntensity
}

Math {
    NonLocal "NLM" (Electrode="top_schottky" Length=2e-6 Digits=3 EnergyResolution=0.001)

        Extrapolate
        Digits= 7
        ErrEff(electron)= 1e-12
        ErrEff(hole)= 1e-12
        RHSmax= 1e30
        RHSmin= 1e-15
        CdensityMin= 1.e-30
        Notdamped= 20
        Iterations= 15
        eMobilityAveraging= ElementEdge
        hMobilityAveraging= ElementEdge
        GeometricDistances
        ParameterInheritance= Flatten
}

Solve {
        Poisson
        Coupled (Iterations=100 LineSearchDamping=1e-4) { Poisson Electron }
        Coupled (Iterations=100 LineSearchDamping=1e-4) { Poisson Electron Hole }

    # IV from 0 to -20V
    Quasistationary (Initialstep= 1e-3 Increment= 1.1 Maxstep= 0.2 Minstep= 1.e-15
                Goal { Name="top_schottky" Voltage=-20 })
        { Coupled { Poisson Electron Hole } }

    # IV from 0 to 5V
    NewCurrentFile= "IV_"
    Quasistationary (Initialstep= 1e-3 Increment= 1.1 Maxstep= 0.025 Minstep= 1.e-15
                Goal { Name="top_schottky" Voltage= 2 })
    { Coupled { Poisson Electron Hole }
        CurrentPlot ( Time= (Range= (0.00 0.50) Intervals= 20; Range= (0.50 0.75) Intervals= 20;
Range= (0.75 1.00) Intervals= 10))
  }
}
```

Appendix 3: TCAD Code for C-V Simulation

```
*****CV simulation-sdevice code****
*********************************************
*******************Device*******************
Device GaNCV {
        Electrode {
                { Name="top_schottky" Schottky Barrier= 0.75 Voltage= 0.0 }
                { Name="bot_ohmic" Voltage= 0.0 Resist=10 }
        }

        File {
                Grid= "@tdr@"
                Plot= "@tdrdat@"
                Current= "@plot@"
                Parameter= "@parameter@"
        }

        Physics {
                Temperature= 300
                AreaFactor= 39250
                Recombination (
                        Radiative
                        SRH(
                                DopingDependence
                                TempDependence
                                # ElectricField(Lifetime=Hurkx DensityCorrection=None)
                        )
                        Auger
                        #Avalanche (vanOverstraetendeMan)
                )

                eBarrierTunneling "NLM"

                Mobility (
                   ConstantMobility
                   #DopingDependence(Masetti)
                   HighFieldSaturation
             )

                EffectiveIntrinsicDensity ( OldSlotboom NoFermi )
        }

        Physics (Region= "EpiSubRegion"){
         Traps (
     (hNeutral Conc=2.4e14 Level EnergyMid=0.55 fromValBand hXSection=2.7e-12 hGfactor=1
hJfactor=0 hConstEmissionRate=0)
     (hNeutral Conc=2.7e14 Level EnergyMid=0.65 fromValBand hXSection=1.7e-14 hGfactor=1
hJfactor=0 hConstEmissionRate=0)
     (hNeutral Conc=4.4e14 Level EnergyMid=0.85 fromValBand hXSection=1.8e-13 hGfactor=1
hJfactor=0 hConstEmissionRate=0)
     (hNeutral Conc=4.1e15 Level EnergyMid=1.20 fromValBand hXSection=4.7e-14 hGfactor=1
hJfactor=0 hConstEmissionRate=0)
     (eNeutral Conc=1.0e14 Level EnergyMid=0.17 fromCondBand eXSection=2.3e-17 eGfactor=1
eJfactor=0 eCOnstEmissionRate=0)
     (eNeutral Conc=9.0e14 Level EnergyMid=0.52 fromCondBand eXSection=3.3e-16 eGfactor=1
eJfactor=0 eCOnstEmissionRate=0)
```

```
    (eNeutral Conc=5.8e14 Level EnergyMid=0.53 fromCondBand eXSection=3.3e-17 eGfactor=1
eJfactor=0 eCOnstEmissionRate=0)
    (eNeutral Conc=5.8e14 Level EnergyMid=0.94 fromCondBand eXSection=1.0e-16 eGfactor=1
eJfactor=0 eCOnstEmissionRate=0)
    )
        Optics (OpticalGeneration (SetConstant (Value= 1e12)))
        }
}
********************End of Device*******************
***************************************************
Plot {
        eDensity hDensity
        eMobility hMobility
        eVelocity hVelocity
        eCurrent hCurrent
        #eQuasiFermi hQuasiFermi
        #egradQuasiFermi hgradQuasiFermi
        Doping
        DonorConcentration
        AcceptorConcentration
        ElectricField
        Potential
        #SpaceCharge
        #ConductionBandEnergy
        ValenceBandEnergy
        #BandGap
        #RadiativeRecombination
        #SRH
        #SRHRecombination
        #Auger
        # AvalancheGeneration
        # eAvalanche hAvalanche
        # OpticalGeneration
        # OpticalIntensity
        #eBarrierTunneling

        #JC: View nonlocal mesh in TDR file
        NonLocal
}
***************************************************
Math {
    NonLocal "NLM" (Electrode="top_schottky" Length=2e-6 Digits=3 EnergyResolution=0.001)

        Extrapolate
        Digits= 7
        ErrEff(electron)= 1e-12
        ErrEff(hole)= 1e-12
        RHSmax= 1e30
        RHSmin= 1e-15
        CdensityMin= 1.e-30
        Notdamped= 20
        Iterations= 15
        eMobilityAveraging= ElementEdge
        hMobilityAveraging= ElementEdge
        GeometricDistances
        ParameterInheritance= Flatten
```

```
        Method= Blocked
        SubMethod= Pardiso
}
**************************************************
File {
        Output= "@log@"
        ACExtract= "@acplot@"
}
**************************************************
System {
        GaNCV cvcurve (top_schottky=1 bot_ohmic=2)
        Vsource_pset vs (1 0) {dc=0}
        Vsource_pset vd (2 0) {dc=0}
}
**************************************************
Solve {
        Coupled (Iterations=100 LineSearchDamping=1e-4) {Poisson}
        Coupled { Poisson Electron }
        Coupled { Poisson Electron Hole }

    # Schottky from 0 to -20V
    Quasistationary (
        Initialstep= 1e-3
        Increment= 1.1
        Maxstep= 0.1
        Minstep= 1.e-15
                Goal { Parameter= vs.dc  Voltage= -20 }
        ) {
                Coupled { Poisson Electron Hole }
        }

        Plot(FilePrefix= "n@node@_vn15")

    # Schottky from -15 to 0V
    NewCurrentFile= "AC_"
    Quasistationary (
        Initialstep= 1e-5
        Increment= 1.1
        Maxstep= 0.1
        Minstep= 1.e-15
                Goal { Parameter= vs.dc  Voltage= 0 }
        ) {
                ACCoupled (
                StartFrequency= 1e6
                EndFrequency= 1e6
                NumberOfPoints= 1
                Decade
                Node(1 2)
                Exclude(vs vd)
        )
        {Poisson Electron Hole}
        Plot (Time= (0; 0.1; 0.2; 0.3; 0.4; 0.5; 0.6; 0.7; 0.8; 0.9) NoOverwrite)
    }
}
******************End of file******************
```

Appendix 4: TCAD Code for Transient Current Simulation

TCAD-TRANSIENT CURRENT FILE:

```
*****Transient current generated by incident ion*****
File {
        Grid= "@tdr@"
        Parameter= "@parameter@"
        Plot= "@tdrdat@"
        Current= "@plot@"
        Output= "@log@"

}

Electrode {
        { Name="top_schottky" Schottky Barrier= 0.75 Voltage= (0.0 at -1, -18 at 0) }
        { Name="bot_ohmic" Voltage= 0.0  Resist=10}
}

Physics {
    Temperature= 300
    AreaFactor=1
        Recombination (
        Radiative
        SRH(
          DopingDependence
          TempDependence
          #ElectricField(Lifetime=Hurkx DensityCorrection=None)
          )
        Auger
        #Avalanche (vanOverstraetendeMan)
        )

        eBarrierTunneling "NLM"

        Mobility (
          ConstantMobility
          #DopingDependence(Masetti)
          HighFieldSaturation(ElectricField)
    )

        EffectiveIntrinsicDensity ( OldSlotboom NoFermi )

        HeavyIon(
        Location=(10, 0, 0)
        Direction=(0, 1, 0)
        Time=1e-15
        Length=[1 2 5 9 11 12 13 14 15]
        Wt_hi=[0.285 0.3 0.33 0.39 0.48 0.54 0.6 0.51 0.18]
        LET_f=[0.0095 0.01 0.011 0.013 0.016 0.018 0.02 0.017 0.006]
        Gaussian
        PicoColumb
        )
}

Physics (Region= "EpiSubRegion") {
    Traps (
```

```
    (hNeutral Conc=2.4e14 Level EnergyMid=0.55 fromValBand hXSection=2.7e-12 hGfactor=1
hJfactor=0 hConstEmissionRate=0)
    (hNeutral Conc=2.7e14 Level EnergyMid=0.65 fromValBand hXSection=1.7e-14 hGfactor=1
hJfactor=0 hConstEmissionRate=0)
    (hNeutral Conc=4.4e14 Level EnergyMid=0.85 fromValBand hXSection=1.8e-13 hGfactor=1
hJfactor=0 hConstEmissionRate=0)
    (hNeutral Conc=4.1e15 Level EnergyMid=1.20 fromValBand hXSection=4.7e-14 hGfactor=1
hJfactor=0 hConstEmissionRate=0)
    (eNeutral Conc=1.0e14 Level EnergyMid=0.17 fromCondBand eXSection=2.3e-17 eGfactor=1
eJfactor=0 eCOnstEmissionRate=0)
    (eNeutral Conc=9.0e14 Level EnergyMid=0.52 fromCondBand eXSection=3.3e-16 eGfactor=1
eJfactor=0 eCOnstEmissionRate=0)
    (eNeutral Conc=5.8e14 Level EnergyMid=0.53 fromCondBand eXSection=3.3e-17 eGfactor=1
eJfactor=0 eCOnstEmissionRate=0)
    (eNeutral Conc=5.8e14 Level EnergyMid=0.94 fromCondBand eXSection=1.0e-16 eGfactor=1
eJfactor=0 eCOnstEmissionRate=0)
    )
    Optics (OpticalGeneration (SetConstant (Value= 1e12)))
}


Plot {
    eDensity hDensity
        eMobility hMobility
        eVelocity hVelocity
        eCurrent hCurrent
        #eQuasiFermi hQuasiFermi
        #egradQuasiFermi hgradQuasiFermi
        Doping
        DonorConcentration
        AcceptorConcentration
        ElectricField
        Potential
        SpaceCharge
        #ConductionBandEnergy
        #ValenceBandEnergy
        #BandGap
        #RadiativeRecombination
        #SRH
        #SRHRecombination
        #Auger
        #AvalancheGeneration
        #eAvalanche hAvalanche
        #OpticalGeneration
        #OpticalIntensity

        HeavyIonCharge
        HeavyIonChargeDensity
        HTrappedCharge
}

Math {
    NonLocal "NLM" (Electrode= "top_schottky" Length= 2e-6 Digits= 3 EnergyResolution= 0.001)
        Extrapolate
        Digits= 7
        ErrEff(electron)= 1e-12
```

```
            ErrEff(hole)= 1e-12
            RHSmax= 1e30
            RHSmin= 1e-15
            CdensityMin= 1.e-30
            Notdamped= 20
            Iterations= 15
            eMobilityAveraging= ElementEdge
            hMobilityAveraging= ElementEdge
            GeometricDistances
            ParameterInheritance= Flatten

            NumberOfThreads= 4
}

Solve {
     Coupled (Iterations=1000 LineSearchDamping=1e-4) {Poisson}
     Coupled {Poisson Electron}
     Coupled {Poisson Electron Hole}

    *ramp Schottky from 0V to -20V
     NewCurrentPrefix="RampV_"
     Transient(
       InitialTime=-1
       FinalTime=0
       InitialStep=1e-3
       MaxStep=0.1
       MinStep=1e-4
       Increment=1.1
       Decrement=2
       AcceptNewtonParameter(ReferenceStep=1e-12)
       )
       {Coupled {poisson electron hole}}

    *maintain Schottky at- 20V, record the transient current generated by incident ion
       NewCurrentPrefix="Transient_"
     Transient(
       InitialTime=0.0
       FinalTime=2e-9
       InitialStep=1e-15
       MaxStep=5e-11
       MinStep=1e-18
       Increment=1.1
       Decrement=2
       AcceptNewtonParameter(ReferenceStep=1e-12)
       )
       {Coupled {poisson electron hole}}
}
```

Appendix 5: TCAD Code for Carrier Concentration Simulation

```
*****Carrier concentration at different times after an incident ion*****
File {
        Grid= "@tdr@"
        Parameter= "@parameter@"
        Plot= "@tdrdat@"
        Current= "@plot@"
        Output= "@log@"

}

Electrode {
        { Name="top_schottky" Schottky Barrier= 0.75 Voltage= (0.0 at -1, -160 at 0) }
        { Name="bot_ohmic" Voltage= 0.0 }
}

Physics {
        Temperature= 300
        AreaFactor=39250
        Recombination (
        Radiative
        SRH(
          DopingDependence
          TempDependence
          # ElectricField(Lifetime=Hurkx DensityCorrection=None)
          )
        Auger
        #Avalanche (Okuto Eparallel)
        )

        eBarrierTunneling "NLM"

        Mobility (
          ConstantMobility
          #DopingDependence(Masetti)
          HighFieldSaturation
    )

        EffectiveIntrinsicDensity ( OldSlotboom NoFermi )

        HeavyIon(
        Location=(10, 0, 0)
        Direction=(0, 1, 0)
        Time=1e-15
        Length=[1 2 5 9 11 12 13 14 15]
        Wt_hi=[0.285 0.3 0.33 0.39 0.48 0.54 0.6 0.51 0.18]
        LET_f=[0.0095 0.01 0.011 0.013 0.016 0.018 0.02 0.017 0.006]
        Gaussian
        PicoColumb
        )
}

Physics (Region= "EpiSubRegion") {
      Traps (
      (hNeutral Conc=2.4e14 Level EnergyMid=0.55 fromValBand hXSection=2.7e-12 hGfactor=1
hJfactor=0 hConstEmissionRate=0)
```

```
    (hNeutral Conc=2.1e14 Level EnergyMid=0.65 fromValBand hXSection=1.7e-14 hGfactor=1
hJfactor=0 hConstEmissionRate=0)
    (hNeutral Conc=3.4e14 Level EnergyMid=0.85 fromValBand hXSection=1.8e-13 hGfactor=1
hJfactor=0 hConstEmissionRate=0)
    (hNeutral Conc=2.9e15 Level EnergyMid=1.20 fromValBand hXSection=4.7e-14 hGfactor=1
hJfactor=0 hConstEmissionRate=0)
    (eNeutral Conc=1.0e14 Level EnergyMid=0.17 fromCondBand eXSection=2.3e-17 eGfactor=1
eJfactor=0 eCOnstEmissionRate=0)
    (eNeutral Conc=9.0e14 Level EnergyMid=0.52 fromCondBand eXSection=3.3e-16 eGfactor=1
eJfactor=0 eCOnstEmissionRate=0)
    (eNeutral Conc=5.8e14 Level EnergyMid=0.53 fromCondBand eXSection=3.3e-17 eGfactor=1
eJfactor=0 eCOnstEmissionRate=0)
    (eNeutral Conc=5.8e14 Level EnergyMid=0.94 fromCondBand eXSection=1.0e-16 eGfactor=1
eJfactor=0 eCOnstEmissionRate=0)
    )
    Optics (OpticalGeneration (SetConstant (Value= 1e12)))
}


Plot {
    eDensity hDensity
        eMobility hMobility
        eVelocity hVelocity
        eCurrent hCurrent
        eQuasiFermi hQuasiFermi
        egradQuasiFermi hgradQuasiFermi
        Doping
        DonorConcentration
        AcceptorConcentration
        ElectricField
        Potential
        SpaceCharge
        ConductionBandEnergy
        ValenceBandEnergy
        BandGap
        RadiativeRecombination
        SRH
        SRHRecombination
        Auger
        #AvalancheGeneration
        #eAvalanche hAvalanche
        #OpticalGeneration
        #OpticalIntensity

        HeavyIonCharge
        HeavyIonChargeDensity
}

Math {
        NonLocal "NLM" (
                Electrode= "top_schottky"
                Length= 2e-6
                Digits= 3
                EnergyResolution= 0.001
        )
        Extrapolate
```

```
            Digits= 7
            ErrEff(electron)= 1e-12
            ErrEff(hole)= 1e-12
            RHSmax= 1e30
            RHSmin= 1e-15
            CdensityMin= 1.e-30
            Notdamped= 20
            Iterations= 15
            eMobilityAveraging= ElementEdge
            * uses edge mobility instead of element one for electron mobility
            hMobilityAveraging= ElementEdge
            * uses edge mobility instead of element one for hole mobility
            GeometricDistances
            * when needed, compute distance to the interface instead of closest
            * point on the interface
            ParameterInheritance= Flatten
            * regions inherit parameters from materials
}

Solve {
    Poisson
    Coupled {Poisson Electron}
    Coupled {Poisson Electron Hole}

     NewCurrentPrefix="RampV_"
     Transient(
     InitialTime=-1
     FinalTime=0
     InitialStep=1e-3
     MaxStep=0.1
     MinStep=1e-5
     Increment=1.1
     Decrement=2
     AcceptNewtonParameter(ReferenceStep=1e-12)
     )
     {Coupled {poisson electron hole}}

     NewCurrentPrefix="Transient_"
     Transient(
     InitialTime=0.0
     FinalTime=5e-10
     InitialStep=1e-15
     MaxStep=5e-11
     MinStep=1e-15
     Increment=1.1
     Decrement=2
     AcceptNewtonParameter(ReferenceStep=1e-12)
     )
     {Coupled {poisson electron hole}
      Plot ( FilePrefix="n30_CarrierDensity_" Time = ( 1e-14; 1e-13; 1e-12; 5.2e-12; 1e-11; 1e-10; 1e-9)
NoOverwrite)
     }
}
```

DEPARTMENT OF DEFENSE

DEFENSE THREAT REDUCTION
AGENCY
8725 JOHN J. KINGMAN ROAD
STOP 6201
FORT BELVOIR, VA 22060
ATTN: D. PETERSEN

DEFENSE TECHNICAL
INFORMATION CENTER
8725 JOHN J. KINGMAN ROAD,
SUITE 0944
FT. BELVOIR, VA 22060-6201
ATTN: DTIC/OCA

DEPARTMENT OF DEFENSE CONTRACTORS

QUANTERION SOLUTIONS, INC.
1680 TEXAS STREET, SE
KIRTLAND AFB, NM 87117-5669
ATTN: DTRIAC